Pergamon

Geochimica et Cosmochimica Acta, Vol. 66, No. 7, pp. 1285–1303, 2002

0016-7037/02 $22.00 + .00

PII S0016-7037(00)00847-X

Two populations of carbonate in ALH84001: Geochemical evidence for discrimination and genesis

JOHN M. EILER,[1,*] JOHN W. VALLEY,[2] COLIN M. GRAHAM,[3] and JOHN FOURNELLE[2]

[1]Geological and Planetary Sciences, Caltech, Pasadena, CA 91125, USA [2]Geology and Geophysics, University of Wisconsin, Madison, WI 53706, USA [3]Geology and Geophysics, University of Edinburgh, Edinburgh, EH9 3JW, Scotland, United Kingdom

(*Received May* 2, 2001; *accepted in revised form October* 10, 2001)

Abstract—We present major and trace-element, oxygen isotope, textural, and structural data for carbonates and related phases in the SNC meteorite ALH84001. These data document the existence of at least two distinct carbonate populations: one composed of finely zoned, chemically and isotopically heterogeneous concretions of magnesio-siderite with distinct white magnesite rims, and a second composed of relatively homogeneous, isotopically and compositionally simple domains of ankeritic carbonate and intimately intergrown glass and fine-grained pyroxene. We suggest on the basis of textural evidence and geochemical systematics that the first population consists of low-temperature aqueous precipitates, and the second is produced by shock melting of the first. Values of $\delta^{18}O$ and Sr/Ca ratios are correlated with one another in magnesio-siderite concretions; the trend formed by these data is consistent with the predicted relationship for inorganic precipitation of carbonate from a solution of constant composition between temperatures of ~190°C (for concretion cores) to 20°C (for magnesite-rich concretion rims). Given the assumptions inherent in this temperature estimate, the aqueous fluid parental to carbonate concretions is constrained to have a $\delta^{18}O$ of −5‰ VSMOW (significantly mass fractionated compared with expected juvenile martian volatiles) and minor-element abundances broadly similar to terrestrial seawater. *Copyright © 2002 Elsevier Science Ltd*

1. INTRODUCTION

The SNC meteorites are a group of 19 achondrites believed to come from the crust of Mars (McSween, 1985, 1994). Several of the SNCs contain carbonates suspected to have formed on the martian surface or in the martian crust (Carr et al., 1985; McSween, 1985, 1994; Gooding et al., 1991; Mittlefehldt, 1994; Wentworth and Gooding, 1994). Carbonate in ALH84001 is distinctive when compared with that in other SNCs in the following respects: its host rock is unusually old (4.5 Ga; Nyquist et al., 1995, vs. <1.3 Ga for other SNCs; McSween, 1994); it is relatively abundant (~1 vol%; Mittlefehldt, 1994; Treiman, 1995); it typically has an unusual disk-shaped or "pancake" morphology (Mittlefehldt, 1994; Romanek et al., 1994; Treiman, 1995; Scott et al., 1997; Scott, 1999, and references therein); there are virtually no recognized coexisting hydrous phases (Mittlefehldt, 1994; Treiman, 1995)—in contrast to the "iddingsite"-carbonate assemblages in Lafayette and Nahkla (Gooding et al., 1991; Treiman et al., 1993; Vicenzi et al., 1997); it exhibits a large-range and distinctive covariation in major-element and oxygen-isotope compositions (Mittlefehldt, 1994; Treiman, 1995; Harvey and McSween, 1996; Valley et al., 1997; Leshin et al., 1998; Scott, 1999, and references therein; this article); and several textural, mineralogic, and geochemical features have been suggested to indicate a biologic origin (McKay et al., 1996).

Several mutually exclusive hypotheses have been proposed for the origin of carbonate in ALH84001, including the following: biologic origin (McKay et al., 1996), precipitation from aqueous fluids at low temperatures (~0 to 300°C; Mittlefehldt, 1994; Romanek et al., 1994; Treiman, 1995; Valley et al., 1997; Treiman and Romanek, 1998), precipitation from aqueous solution near 0°C as part of an evaporite sequence (McSween and Harvey, 1998; Warren, 1998), distillation from aqueous or carbonic fluids at or above 300°C (Leshin et al., 1998), precipitation at 150°C and brief heating at ≤470°C (Golden et al., 2001), growth from hot (≥700°C) vapor of unspecified chemistry (Bradley et al., 1996), replacement of mafic silicates during metamorphism at temperatures of ≥650°C (Harvey and McSween, 1996), quenching from mixed silicate–carbonate impact melt, of which coexisting silicate glass is thought to represent a complementary component (Scott et al., 1997), and shock melting of preexisting carbonates (Scott et al., 1998; Scott, 1999). The unusual nature of the minerals in question and the lack of geological context for the sample have made it difficult to reject any of these hypotheses.

We present here a study of the major and trace elements, stable isotope geochemistry, and structural properties of carbonate and related phases in ALH84001. What distinguishes our work from previous studies is its relatively large set of mutually supporting observations of the same portions of the rock. These data test several of the more specific models listed above, suggest a quantitative constraint on the temperature of origin and chemistry of fluids parental to carbonates in this sample, and document new evidence for a second population of carbonate distinct from carbonate concretions that have been the focus of previous studies.

2. CARBONATE PETROGRAPHY

Our analytical work on carbonate and related phases in ALH84001 was accompanied by examination of thin section 311, prepared from potted butt ALH84001.119 (Fig. 1) and polished grain mounts of several other subsamples of ALH84001 by optical, secondary-electron, backscattered-elec-

* Author to whom correspondence should be addressed (eiler@gps.caltech.edu).

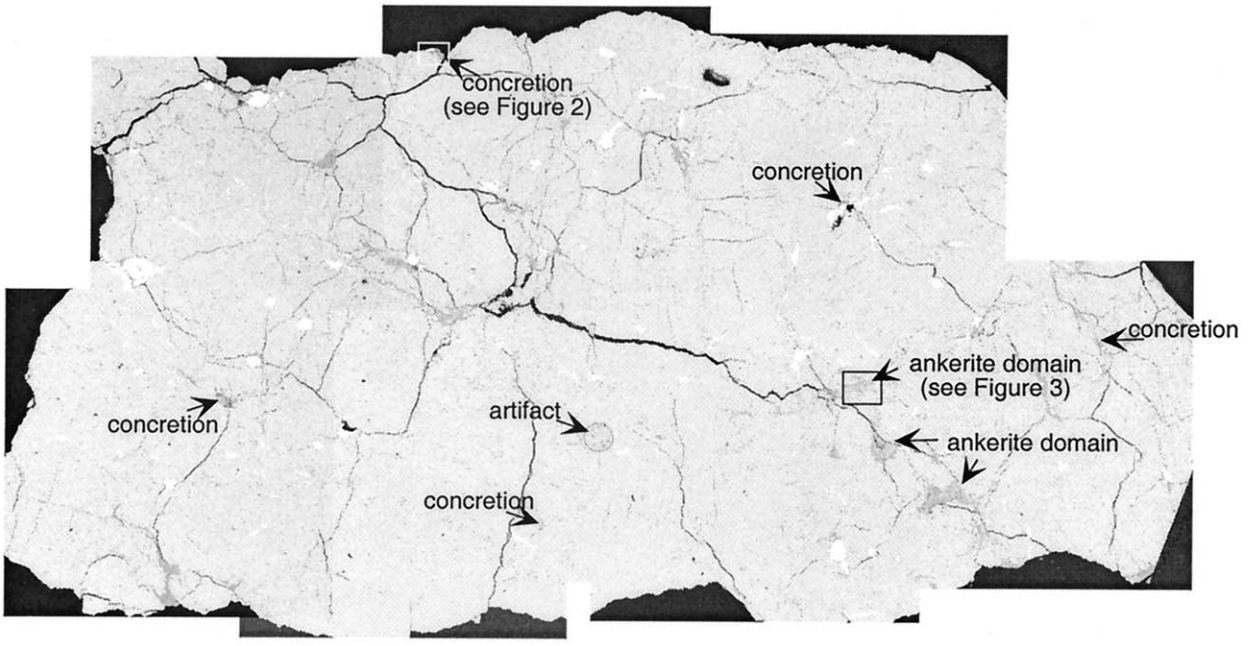

Fig. 1. Photomosaic of backscattered electron images of thin section ALH84001.119. The field of view is approximately 2 cm wide. The light gray, fractured material making up most of the image is ~En_{70} orthopyroxene. Ankerite domains and carbonate concretions (see text and Figs. 2 and 3) that are visible at this scale are labeled. Bright phases are chromite. Most featureless, dark gray phases are feldspathic glass (although Ca phosphates are not easily distinguished from glass in this image). The circular, ~1-mm feature near the center of the field of view is an artifact.

tron, cathodoluminescence, and X-ray mapping. In this section, we summarize the results of these findings with emphasis on observations not previously documented in the literature. For reference, we also provide a brief review of general observations regarding the petrography of carbonate in ALH84001 (McSween, 1994; Mittlefehldt, 1994; Treiman, 1995; Harvey and McSween, 1996; Scott et al., 1997, 1998; Treiman, 1998; Treiman and Romanek, 1998; Scott, 1999). We note at the outset of this discussion that ALH84001 is a petrographically complex specimen and it is possible (even likely) that our observations do not describe the full range of textural relationships observable in other portions of this sample not available for our study.

Carbonate in ALH84001 is present at ~1% abundance (by volume), which we recognize as belonging to four textural types, described in the following paragraphs. Some occurrences of carbonate have been previously described that appear to be modified (i.e., fractured or cross-cut by glass) examples of one of these four populations:

(1) Concretions. The most distinctive and widely discussed carbonate population is disk-shaped concretions (also referred to as "rosettes," "globules," or "pancakes") with estimated dimensions of ~20 to 200 μm in diameter and ~10 to 50 μm thick (Fig. 2). These concretions are concentrated on the surfaces of fractures found throughout this heavily shocked sample and display a distinctive chemical and textural zonation. Most of their volume is made up of a core of carbonate that appears orange in hand-sample and thin section and contains trace inclusions of FeS (Shearer et al., 1996) and magnetite (Bradley et al., 1996). Orange cores of carbonate concretions commonly have compositions approximately in the middle of the ankerite/magnesio-siderite solvus but may contain patches of approximately ankeritic composition and, more rarely, small patches of magnesian-calcite composition (Mittlefehldt, 1994; Treiman, 1995; Harvey and McSween, 1996). We are aware of no previous structural characterizations of any of these carbonate populations that uses phase-diagnostic techniques such as X-ray, electron, or neutron diffraction, other than confirmations from transmission electron microscopy measurements that it is rhombohedral carbonate (Bradley et al., 1996). Orange cores are surrounded by a black band, ~5 to 10 μm thick, rich in magnetite inclusions in a carbonate substrate of uncertain chemistry. This black band is surrounded by a white band, ~10 to 15 μm thick, composed of Mg-rich carbonate (also having unknown structural properties). Finally, a second black, inclusion-rich band typically forms the concretion rim. Optically, these carbonates have a radial fibrous texture that cuts across compositional bands.

(2) Small (estimated 20- to 50-μm diameter) concretions cored by white Mg-rich carbonate and surrounded by a black band (i.e., similar to large concretions but smaller and free of the orange carbonate core).

(3) Carbonate veins with the chemical composition and zonation of orange carbonate, but distributed within fine fractures and grain boundaries in the orthopyroxene host rather than as disk-shaped bodies.

(4) Massive domains of ankeritic carbonate, variably intergrown with silicate glass and minerals, larger than concretions, not having a disklike shape, and lacking concentric rims of white, Mg-rich carbonate or black, oxide-rich assemblages. Massive carbonates that may be members of this population have been described previously by Treiman (1998) and Scott

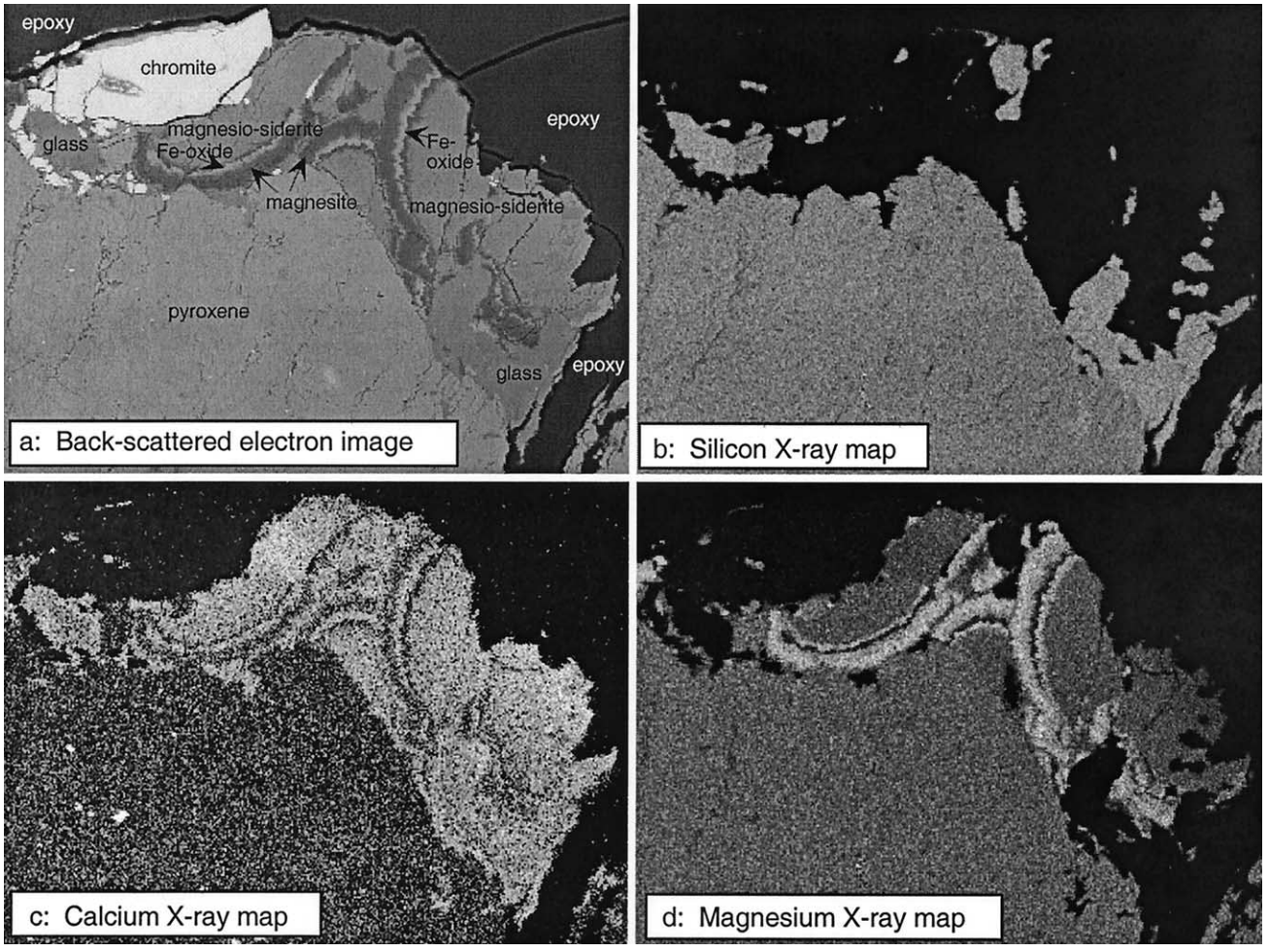

Fig. 2. Backscattered electron image (a) and X-ray maps (b, silicon; c, calcium, d, magnesium) of several large concretions (texture type 1 described in text). Field of view is 580 μm wide. Carbonate is fractured, poor in Ca, and rimmed by magnesite and iron oxide; it displays approximately concentric zoning, including sharp compositional steps. Glass, when present, cross-cuts compositional bands in carbonate; pyroxene encloses carbonate.

(1999). One of the samples on which work for this study was done (thin section 311 from subsample ALH84001.119) contains several large (~500- to 1000-μm diameter) domains of ankeritic carbonate intimately intergrown with fragments of orthopyroxene and rounded patches of feldspathic glass (Fig. 3). Three of these domains are linked to one another by a network of fractures with right-lateral steps or kinks where the fractures intersect each domain of ankeritic carbonate (Fig. 1, lower right). Feldspathic glass has an unusual textural relationship to this type of carbonate: it is abundant and present as isolated spheroids or clusters of spheroids (Fig. 3). These textures suggest that carbonate and enclosed glass formed contemporaneously, in contrast to the veins of feldspathic glass that sometimes cross cut, and are thus younger than, carbonate concretions (e.g., right-hand side of Fig. 2). Ca-poor carbonates are occasionally found along the margins of, or near inclusions within, these large ankeritic domains, but unlike concretions, this association is not ubiquitous and displays no textural organization (i.e., most massive ankerite is in direct contact with orthopyroxene or glass without zoned, Ca-poor carbonate in an intermediate position). Finally, orthopyroxenes associated with ankerite domains are present not only as an enclosing matrix phase but also as abundant isolated, equant grains or "clots" of small equant grains surrounded by carbonate on all visible sides.

Similarities among the first three textural types described above are sufficiently great that we consider them members of the same carbonate population. However, we compare and contrast carbonate "concretions" (textural type 1; Fig. 2) and ankerite-rich domains (textural type 4; Fig. 3). These two populations have some properties in common. Regions of carbonate having chemical zonation resembling concretions are occasionally observed along the edges of, or as inclusions in, some ankeritic domains; similarly, the major-element chemistry of Ca-rich cores of carbonate concretions are ankeritic in some instances (Harvey and McSween, 1996). However, the differences between these populations are more marked, including contrasts in their typical scale (~100 μm for concretions; ~500 to 1000 μm for ankerite-rich domains), in their pattern and degree of chemical zonation (compositionally extreme, fine-scale, and radial zonation in concretions—Harvey and McSween, 1996; Fisler and Cygan, 1998; Fig. 2 and data

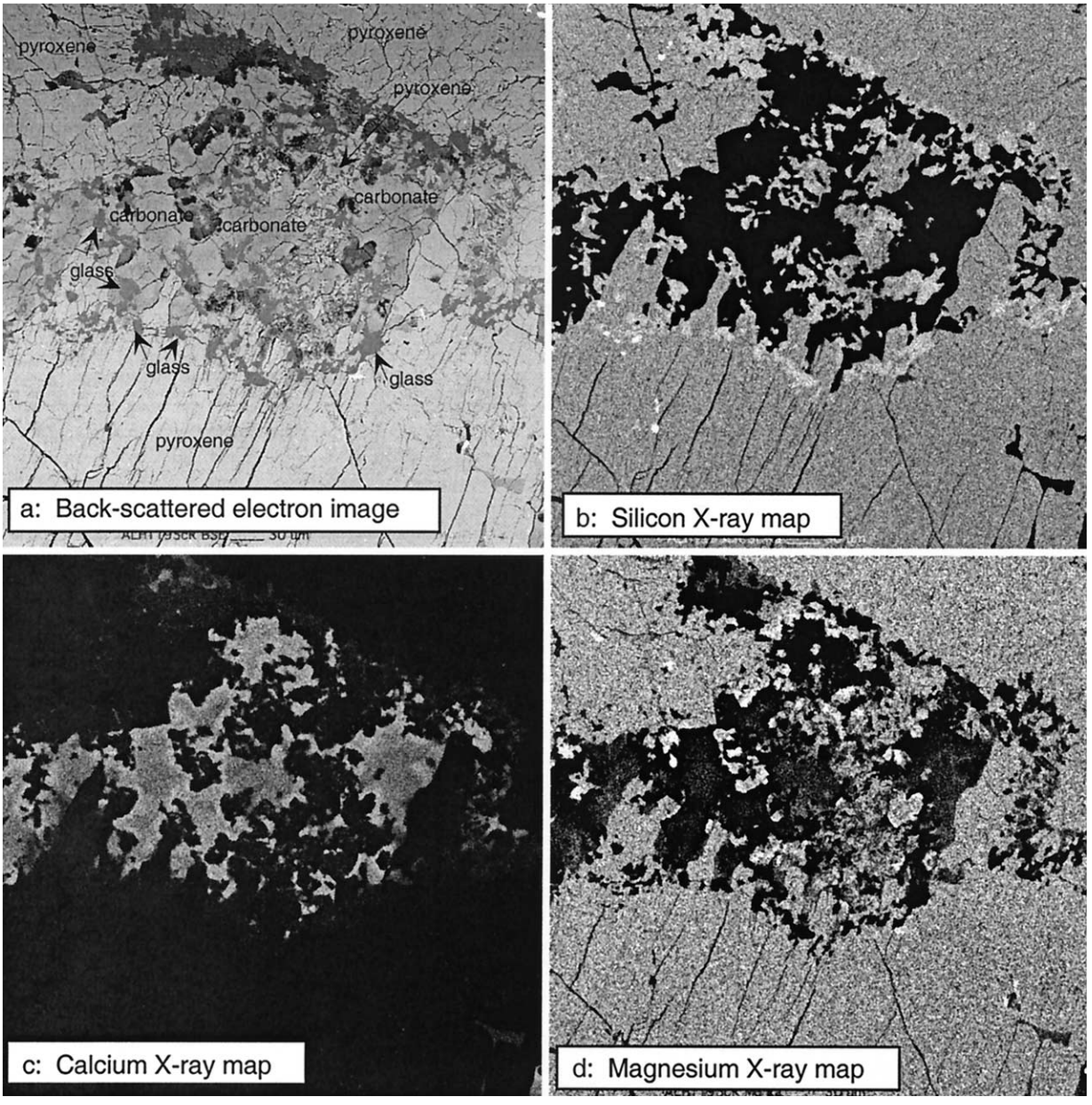

Fig. 3. Backscattered electron image (a) and X-ray maps (b, silicon; c, calcium; d, magnesium) of an ankerite domain (texture type 4 described in text). The field of view is 500 μm wide. Carbonate is rich in Ca, lacks continuous rims of magnesite or iron oxide, and displays only patchy, gradiational compositional zoning. Glass is ubiquitous as abundant, rounded, equant inclusions in carbonate. Pyroxene encloses carbonate but is also present as abundant inclusions of fine tabular grains and clots of fine tabular grains.

discussed below; subtle, gradational, and patchy zonation in ankeritic domains—Fig. 3 and data discussed below) and in their textural relationships to feldspathic glass and pyroxenes. For this reason, we organize the chemical and isotopic data in the following sections to draw particular attention to similarities and differences between these two texturally defined populations of carbonate.

3. CARBONATE MAJOR-ELEMENT CHEMISTRY

We analyzed the major-element (Ca, Mg, Mn, Fe) compositions of 71 spots of carbonate in ALH84001 by electron microprobe; these data are presented in Table 1. These measurements are based exclusively on wavelength-dispersive analysis; we used techniques summarized in the Appendix. All analytical spots were chosen on the basis of images of BSE and X-ray maps of Si, Mg, Ca, Fe, and C. Figure 4 presents the results of these measurements projected from $MnCO_3$ onto the $CaCO_3$-$MgCO_3$-$FeCO_3$ plane (i.e., comparable to Fig. 1 of Harvey and McSween, 1996). Our results generally confirm previously observed chemical variations in carbonate in ALH84001 and in particular support previous evidence for the predominance of carbonate compositions far removed from

Table 1. Major-element analyses of ALH84001 carbonates.

	Mole fraction			
Region	$CaCO_3$	$MgCO_3$	$FeCO_3$	$MnCO_3$
1	0.053	0.862	0.083	0.003
1	0.054	0.784	0.160	0.002
1	0.058	0.811	0.127	0.004
1	0.059	0.743	0.194	0.004
1	0.082	0.618	0.295	0.005
1	0.092	0.591	0.312	0.004
1	0.116	0.559	0.315	0.009
1	0.139	0.507	0.338	0.017
2	0.144	0.481	0.351	0.024
2	0.153	0.460	0.354	0.034
2	0.222	0.421	0.315	0.042
2	0.225	0.439	0.298	0.038
2	0.254	0.413	0.286	0.046
2	0.270	0.393	0.283	0.053
2	0.299	0.413	0.249	0.040
2	0.415	0.350	0.184	0.051
2	0.444	0.340	0.163	0.053
2	0.447	0.349	0.157	0.047
2	0.469	0.327	0.147	0.057
2	0.479	0.333	0.137	0.051
2	0.507	0.297	0.131	0.065
2	0.538	0.275	0.119	0.068
2	0.654	0.197	0.083	0.067
2	0.681	0.168	0.076	0.075
3	0.035	0.953	0.011	0.001
3	0.038	0.940	0.021	0.000
3	0.040	0.900	0.059	0.001
3	0.053	0.713	0.226	0.009
3	0.056	0.685	0.253	0.006
3	0.075	0.639	0.282	0.005
3	0.083	0.611	0.301	0.006
3	0.612	0.216	0.099	0.074
4	0.225	0.420	0.313	0.043
5-I	0.303	0.411	0.242	0.044
5-I	0.309	0.414	0.235	0.042
5-I	0.443	0.349	0.160	0.049
5-I	0.453	0.340	0.152	0.055
5-I	0.489	0.308	0.142	0.061
5-II	0.457	0.338	0.154	0.051
5-II	0.503	0.312	0.127	0.057
5-II	0.525	0.280	0.125	0.070
5-II	0.577	0.242	0.107	0.075
5-II	0.579	0.243	0.103	0.075
5-II	0.592	0.233	0.103	0.072
5-II	0.620	0.218	0.089	0.074
5-II	0.650	0.197	0.081	0.072
5-II	0.674	0.179	0.074	0.074
5-II	0.706	0.153	0.061	0.080
8	0.097	0.574	0.324	0.005
8	0.107	0.556	0.330	0.007
11	0.049	0.783	0.165	0.004
11	0.051	0.818	0.127	0.004
11	0.063	0.698	0.234	0.005
11	0.086	0.607	0.303	0.004
11	0.090	0.600	0.307	0.003
12	0.072	0.733	0.191	0.004
13	0.098	0.570	0.328	0.004
13	0.098	0.578	0.318	0.006
13	0.104	0.565	0.322	0.008
13	0.105	0.578	0.314	0.004
13	0.135	0.503	0.353	0.009

(Continued)

Table 1. (Continued)

14	0.048	0.821	0.128	0.002
14	0.055	0.790	0.152	0.003
14	0.091	0.599	0.307	0.004
14	0.104	0.570	0.320	0.006
14	0.113	0.553	0.325	0.009
15	0.044	0.903	0.052	0.001
15	0.048	0.800	0.149	0.003
15	0.089	0.584	0.323	0.004
15	0.090	0.598	0.308	0.003
15	0.098	0.579	0.315	0.007

stoichiometric calcite, stable dolomite/ankerite solid solutions, or stable magnesite/siderite solid solutions (McSwiggen, 1993; Davidson, 1994). The significance of compositions within the two carbonate solvi has been discussed previously (Treiman, 1995; Valley et al., 1997; Treiman and Romanek, 1998) and will be considered in detail below. The data reported here form a more coherent compositional trend than previously observed (i.e., departures from a line of interpolation through these data are smaller than in previous data sets). This might reflect simpler compositional systematics in the carbonate population we have analyzed as compared with carbonate in ALH84001 generally and/or greater analytical uncertainties of EDS measurements used in some previous studies compared with wavelength-dispersive analysis measurements reported here. It may also reflect the use of imaging to guide quantitative analysis, which allowed us to avoid cracks, inclusions, and impurities. It has been previously suggested that major element compositions of carbonates in ALH84001 vary continuously (if complexly) from Ca-rich to Ca-poor compositions (e.g., Mittlefehldt, 1994; Treiman, 1995; Harvey and McSween, 1996; Valley et al., 1997; Leshin et al., 1998). Although the data in Figure 4 could be interpreted in this way, the character of these variations differs among various textural and compositional subsets. Most markedly, Ca-poor carbonates from concretions (unfilled symbols) vary complexly and continuously in interelement ratios for all plotted components (i.e., Fe/Mg, Ca/Mg, and Ca/Fe), whereas Ca-rich carbonates from ankerite domains (black symbols) vary greatly in Ca content but are approximately constant in Fe/Mg ratio (i.e., the projection of the trend for these data intersects the $CaCO_3$ apex). Furthermore, there is a gap be-

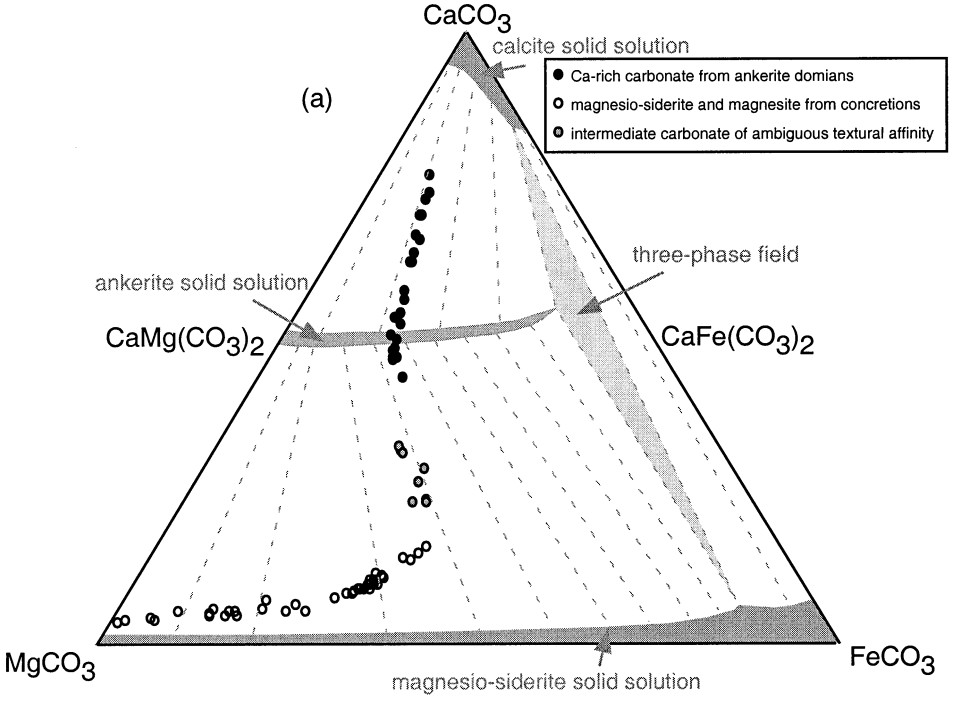

Fig. 4. Major-element compositions of carbonates in thin section ALH84001.119, as determined by wavelength-dispersive analysis electron-microprobe analyses. Data are plotted as molar abundances of Ca, Mg, and Fe carbonate end members, projected from $MnCO_3$; open circles are carbonate in concretions (Fig. 2); solid circles are Ca-rich carbonate that dominates ankerite domains (Fig. 3); gray circles are patches of Ca-poor carbonates occasionally found in or near ankerite domains (these compositions resemble those previously reported for some concretion cores; Harvey and McSween, 1996). Stability fields for Mg-Ca-Fe carbonates at 500°C are shown as gray fields and dashed gray tie lines (after McSwiggen, 1993; these fields are representative of those between 300 and 700°C.

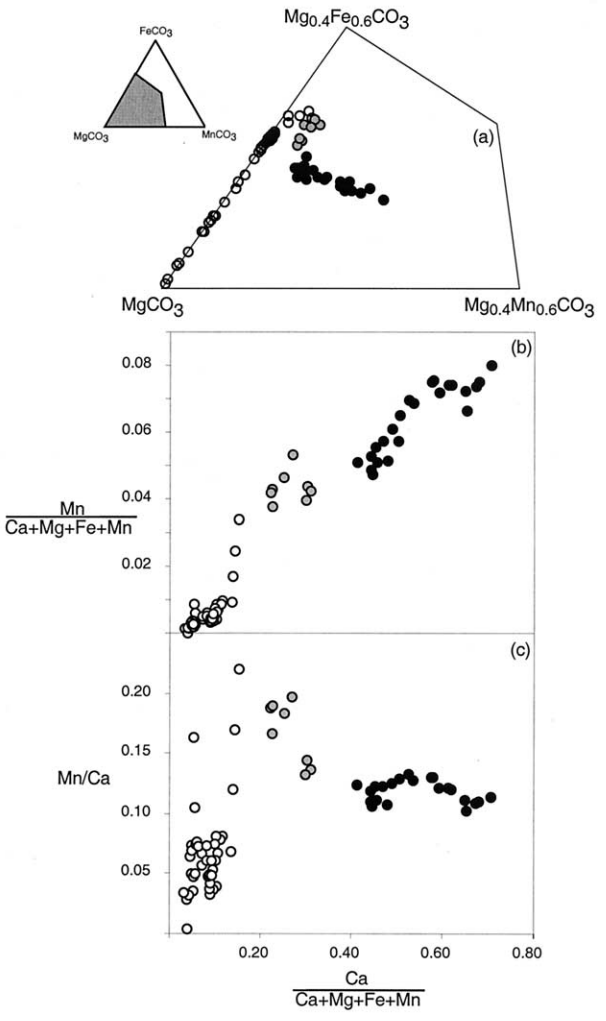

Fig. 5. Systematics of Mn abundance variations in carbonates from ALH84001.119; these data replot results shown in Fig. 4. (a) Molar abundances of Fe, Mg, and Mn carbonate end members, projected from $CaCO_3$. (b) Mn as a fraction of all cations vs. Ca as a fraction of all cations. (c) Mn/Ca ratio vs. Ca as a fraction of all cations. Symbols are as in Figure 4. See text for discussion.

tween these two populations that is only partially "filled" in the plotted dimensions by carbonate with intermediate Ca content found as patches in some ankerite domains (gray symbols) and similar compositions previously reported as a component of some concretions (Harvey and McSween, 1996). In the following section, we consider major-element variations of ALH84001 carbonates from several perspectives to examine whether the populations we identify in Figure 4 form continuous trends in other compositional projections.

Ca-rich carbonates in ALH84001 contain up to 8 mol% $MnCO_3$; we replot our data in the Mg-Fe-Mn carbonate plane (projected from $CaCO_3$) in Figure 5a to illustrate the relationship of Mn contents to concentrations of other elements. As with Figure 4, this plot illustrates that Fe/Mg ratios of ankeritic carbonate are nearly fixed (i.e., the trend for filled circles intersects $MnCO_3$ apex) but, in contrast to Figure 4, Ca-poor carbonates do not form a compositional trend that is continuous with the array for ankerites (i.e., the trend for unfilled and gray symbols varies greatly in Fe/Mg ratio without systematically approaching the array for ankerites). Figures 5b,c further illustrate details of the relationship between Mn and Ca concentrations in ALH84001 carbonates; Figure 5b presents the correlation between Mn and Ca concentrations (as mole fractions of all cations), whereas Figure 5c plots the molar Mn/Ca ratios as a function of the molar Ca/(Ca + Mg + Fe + Mn) ratios. There is in general a positive correlation between Ca and Mn contents among all carbonates in ALH84001 (Fig. 5b), although in detail, Ca-poor carbonates (including all of the carbonate in concretions and patches of Ca-poor carbonate occasionally found in ankeritic domains) form one relatively scattered trend with a high slope, whereas Ca-rich carbonate (making up the main body of ankerite domains and absent in concretions) forms a separate, more well defined trend with a shallower slope. The distinction between these trends is more clear in Figure 5c, which shows that the Mn/Ca ratio is nearly constant over a large range in Ca abundance in Ca-rich carbonates from ankeritic domains but is highly variable and positively correlated with Ca content in Ca-poor carbonates. Collectively, we consider that the compositional systematics illustrated in Figures 4 and 5 suggest at least two distinct groups (whatever their genetic relationship to one another). One group is characterized by nearly fixed Fe/Mg and Mn/Ca ratios (i.e., varying only along the exchange vector $(Fe_{0.3}Mg_{0.7})CO_3$-$(Mn_{0.1}Ca_{0.9})CO_3$), rich in Ca, and dominating ankerite domains, and a second group is characterized by highly variable Fe/Mg and Mn/Ca ratios (i.e., compositional variance in the Mg-Mn-Fe-Ca carbonate system cannot be limited to one vector), poor in Ca, and dominantly composed of carbonate from concretions.

The distinction between Ca-poor and Ca-rich carbonate types in Figure 5c corresponds closely (although not perfectly) to the distinction between concretions and ankerite domains, as defined above on textural grounds alone. For the purposes of further discussion, we define ankeritic carbonates on the basis of major-element chemistry ($X_{CaCO_3} \geq 0.4$ and constant Fe/Mg and Mn/Ca ratios); to first order, this group is equivalent to ankerite domains and these terms will be used interchangeably. Similarly, we define all magnesites and magnesio-siderites ($X_{CaCO_3} < 0.4$) to belong to a single, albeit chemically diverse, group; to first order, this group is equivalent to carbonate concretions and these terms will be used interchangeably.

Concentrations of Mn in carbonate concretions are less than 5 mol% and commonly less than 2 mol% of all cations (Fig. 5b). Such low concentrations have only a small influence on the solvus between dolomite/ankerite and magnesite/siderite solid solutions in the Ca-Mg-Fe system (Essene, 1983) and therefore support previous suggestions (e.g., Valley et al., 1997) that Ca-rich members of this population, which are intermediate between dolomite/ankerite and magnesite/siderite in Ca content, formed metastably with respect to this solvus. However, concentrations of Mn in Ca-rich carbonates that dominate ankerite domains are significantly higher (up to 8 mol% of all cations) and are within the range known to substantially expand solid solution among rhombohedral Ca-Mg-Fe carbonates (Essene, 1983). Mn contents of carbonates in ALH84001 are generally higher by factors of 10 to 20 than coexisting mafic silicates (Treiman, 1995). Given the abundance of carbonate in this sample (~1%), this observation suggests that carbonate cannot have formed by reaction of primary silicate phases with

Table 2. X-ray diffraction data on concretion cores.[a]

d-Spacings of diffraction lines for ALH84001 concretion no:							Reference[d]	
1[b]	2[b]	3[b]	3[c]	4[c]	Average	±SD	Siderite	Intensity
3.590	ND	ND	ND	3.573	3.582	0.008	3.592	25
2.786	2.793	2.788	2.781	2.797	2.789	0.006	2.795	100
2.343	2.338	ND	2.332	2.350	2.341	0.007	2.346	20
2.134	2.126	2.128	2.133	2.135	2.131	0.004	2.134	20
1.972	1.966	1.969	1.965	1.971	1.969	0.003	1.965	20
1.776	ND	ND	ND	1.797	1.787	0.011	1.797	12
1.737	ND	ND	1.737	1.738	1.737	0.000	1.738	30
1.731	1.729	1.731	1.733	ND	1.731	0.001	1.731	35
1.514	1.504	ND	1.501	1.503	1.506	0.005	1.506	14
1.427	ND	ND	1.424	1.424	1.425	0.001	1.427	11
1.354	1.356	ND	1.351	1.354	1.354	0.002	1.355	11

[a] ND = not determined (line obscured or too faint for confident assignment).
[b] Cr source.
[c] Cu source.
[d] Ivigtut siderite; data reported in Mineral Powder Diffraction File Data Book. 1396 pp. Published by JCPDS, International Center for Diffraction Data, Swarthmore PA. P. Bayliss, D. C. Erd, M. E. Mrose, A. P. Sabina and D. K. Smith (eds.). 1986.

solute-poor, CO_2-bearing vapor because those reactions produce secondary silicates (e.g., silica, as by the reaction orthopyroxene + CO_2 = SiO_2 + magnesio-siderite) that are not observed. Carbonate chemistry instead requires that Mn was introduced to the rock as a component of aqueous or supercritical fluid or melt.

4. PHASE IDENTIFICATION

If compositions of concretion cores (Figs. 2, 4) are representative of a single, homogeneous crystalline phase, they violate the equilibrium solvus between magnesio-siderite and dolomite/ankerite at all temperatures and therefore require that carbonate grew and was preserved metastably. This constraint suggests an origin analogous to metastable carbonates in terrestrial environments, which are common as near-surface, low-temperature aqueous precipitates and rare elsewhere (e.g., Curtis et al., 1986; Mozley and Carothers, 1991; Laverne, 1993; Stranger and Neal, 1994; Deelman, 1999). However, on the basis of existing chemical analyses only, it would be possible that these compositions are simply intimate, fine-grained physical mixtures of phases on either side of that solvus. Therefore, a measurement capable of discriminating between such a mixture and a single solid solution provides a test as to whether such compositions do or do not violate the equilibrium solvus.

We determined some of the structural characteristics of concretion cores in ALH84001 by X-ray diffraction analysis of fragments mechanically microsampled from individual concretions by use of a precession Gandolfi camera, and by reflectance Fourier transform infrared (FTIR) analysis of orange concretion cores on fracture surfaces. The analytical techniques and methods of standardization are described in the Appendix.

The d-spacings identified by X-ray diffraction of four individual orange concretion cores (Table 2) are similar to those known for siderite solid solutions and are consistent with unit-cell dimensions of a = b = 4.685 ± 0.003 Å, c = 15.351 ± 0.029 Å, for a cell volume of 291.77 ± 0.59 Å^3. These values are consistent with rhombohedral Ca-Mg-Fe carbonate having the average composition of concretion cores ($\sim Ca_{0.20}Fe_{0.20}Mg_{0.60}CO_3$), assuming linear relationships between the abundance of end member components and unit cell dimensions (Reeder, 1983; Gil et al., 1992). Our measurements show no evidence for a mixture of two rhombohedral carbonates with different unit cell dimensions, which would be revealed by "doublets" for many of the d-spacings listed in Table 2 (e.g., Goldsmith, 1960). In particular, our data are inconsistent with the presence of ankerite/dolomite solid solutions at abundances greater than 4 to 8 mol%, on the basis of the measured intensities of major d-spacings in ankerite and magnesio-siderite standards and the relative intensity of the weakest identified peak observed in our diffraction patterns for ALH84001 carbonate samples. This maximum is insufficient to permit the Ca measured by electron microprobe analysis to be contained in ankerite inclusions within a dominant siderite host (Fig. 4), and thus indicates that siderite must contain most or all of the Ca in solid solution (as is also suggested by the measured unit cell dimensions of that siderite).

Reflectance FTIR measurements of nine orange concretion cores reveal reflectance features at wave numbers of 890.7 ± 1.7 cm^{-1} (resembling the ν_4 peak at ~880 cm^{-1} in carbonate standards) and 748.0 ± 1.8 cm^{-1} (resembling the ν_2 peak at ~730 cm^{-1} in carbonate standards; Table 3). Comparison with physically similar samples of carbonate standards analyzed under the same conditions and with data from previous studies (Adler and Kerr, 1963; Farmer and Warne, 1978; Dubrawski and Channon, 1989; Dubrawski et al., 1989) indicates that these features are consistent with a magnesio-siderite solid solution and inconsistent with other known carbonates in the Ca-Mg-Fe system, including dolomite/ankerite solid solutions. Our observations show no evidence for a mixture of carbonate phases, which is expected to produce doublets or peak broadening at ν_2 and/or ν_4. However, unlike the X-ray diffraction data presented above, we do not believe we can place a strict upper limit on the quantity of a second carbonate phase that might be present as a minor component of magnesio-siderite—these data simply fail to reveal positive evidence for such a component. Our results may conflict with recent RAMAN spectra and FTIR measure-

Table 3. Wave numbers assigned to major features of reflectance FTIR spectra of ALH84001 carbonate concretion cores and carbonate standards.[a]

ALH84001	υ^2	υ^4
Concretion core no.		
1	750.2	892.9
2	750.2	891.0
3	748.2	891.0
4	748.2	889.0
5	746.3	892.9
6	748.2	889.0
7	748.2	892.9
8	744.4	889.0
9	ND	889.0
Average	748.0	890.7
±1SD	1.8	1.7
Reference standards		
Siderite	742.5	878.9
Magnesite	756.0	905.1
Dolomite	734.8	896.7
Ankerite	733.8	893.8
Calcite	715.5	889.5

[a] ND = not determined.

ments of the ~1100 cm^{-1} adsorption feature in the near-rim region of a carbonate concretion in ALH84001 (Cooney et al., 1999), which were interpreted to provide evidence for multiple carbonate phases, submicron-scale compositional heterogeneity, or structural disorder. We do not believe the possible disagreements between these two data sets can be evaluated until more direct comparisons are made (i.e., using measurements of the same portions of the same samples and using the same mineral standards).

In summary, X-ray diffraction and FTIR measurements of concretion cores in ALH84001 are consistent with them being composed entirely of magnesite/siderite solid solution with an intermediate Fe/Mg ratio and expanded unit cell dimensions due to incorporation of Ca in the octahedral site. This result indicates that orange carbonates in ALH84001 are metastable with respect to the magnesio-siderite/ankerite solvus. Note that this constraint does not apply to Ca-rich carbonate that dominates ankerite domains, which is generally closer to pure ankerite in composition and is rich is Mn (which expands all solvi in the Ca-Mg-Fe system of rhombohedral carbonates). We have not been able to identify ankerite domains in bulk samples of ALH84001 and therefore have not subjected them to X-ray diffraction and reflection FTIR studies.

5. OXYGEN ISOTOPES

We report 56 new in situ measurements of $\delta^{18}O$ from 20- to 30-μm spots in carbonates from ALH84001, including a range of ankeritic compositions not well represented in previous studies, and 68 measurements of $\delta^{18}O$ in associated pyroxene (n = 54), oxide (n = 6), and feldspathic glass (n = 8); individual measurements of carbonates are presented in Table 4, and relatively simple results for other phases are only summarized in figures described below. These measurements were made by ion microprobe techniques described in the Appendix. We do not report data for analytical spots that significantly overlapped with adjacent phases or that appeared to have penetrated the target phase and sputtered underlying phases based on examination of the sample with a petrographic microscope and electron microprobe analysis after measurement. Results of accepted measurements for all phases are summa-

Table 4. Oxygen isotope analyses of ALH84001 carbonates.

Region	$CaCO_3$ (mole fraction)	$\delta^{18}O$ (‰)
1	0.05	20.3
1	0.05	22.9
1	0.06	18.5
1	0.06	15.4
1	0.08	19.0
1	0.09	17.1
1	0.12	14.6
1	0.14	10.4
2	0.14	6.9
2	0.22	7.1
2	0.23	3.9
2	0.25	3.5
2	0.27	5.1
2	0.42	4.5
2	0.44	5.1
2	0.48	9.5
2	0.65	5.1
2	0.68	8.8
3	0.04	23.7
3	0.05	13.1
3	0.06	17.1
3	0.08	17.7
3	0.08	17.0
3	0.61	3.1
5-I	0.30	1.7
5-I	0.31	5.3
5-I	0.44	0.3
5-I	0.45	4.5
5-I	0.49	6.3
5-II	0.46	5.7
5-II	0.50	3.3
5-II	0.53	6.7
5-II	0.58	3.5
5-II	0.58	5.9
5-II	0.59	6.0
5-II	0.65	7.0
5-II	0.67	9.1
5-II	0.71	4.7
8	0.10	13.4
8	0.11	14.6
11	0.05	18.2
11	0.05	13.2
11	0.09	14.0
13	0.10	11.7
13	0.10	11.5
13	0.11	13.1
13	0.14	11.3
14	0.05	23.5
14	0.06	26.2
14	0.09	20.7
14	0.10	16.7
15	0.04	26.9
15	0.05	22.4
15	0.09	14.2
15	0.09	17.8
15	0.10	14.0

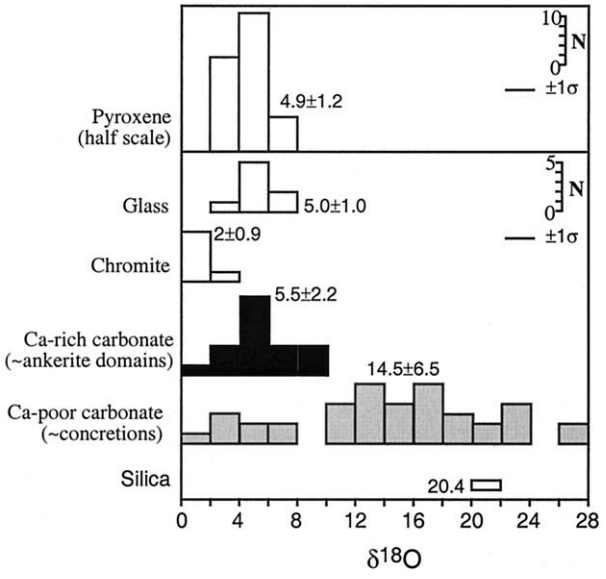

Fig. 6. Summary of oxygen isotope compositions of phases from ALH84001.119 measured by ion microprobe. Silicate and oxide phases are shown in white; Ca-poor carbonate—mostly from concretions—in light gray (note magnesio-siderite cores and magnesite rims are separated from one another for further detail); Ca-rich carbonate from ankerite domains is shown in black. Pyroxene, feldspathic glass, chromite, and Ca-rich carbonates are homogeneous within analytical precision and consistent with mutual high-temperature oxygen isotope equilibrium, whereas Ca-poor carbonates span a wide range in $\delta^{18}O$, most of which is far from high-temperature equilibrium with coexisting phases. The measurement of silica is reproduced from Valley et al. (1997).

rized along with previous data for silica in ALH84001 by using the same laboratory and methods (Valley et al., 1997) in Figure 6 and our new data for carbonates are plotted vs. molar Ca/(Ca + Fe + Mg + Mn) and Mg/(Ca + Fe + Mg + Mn) ratios previously measured for those spots by electron microprobe in Figures 7a,b. Our results confirm the overall trend of $\delta^{18}O$ with chemical composition seen in previous ion microprobe studies (Valley et al., 1997; Leshin et al., 1998; Saxton et al., 1998), in particular showing that $\delta^{18}O$ varies by ~25‰ and tends to decrease with increasing Ca content. However, we have analyzed a larger proportion and wider compositional range of Ca-rich carbonates compared with previous studies, revealing that there are two distinct trends in plots of $\delta^{18}O$ vs. major elements: decreasing $\delta^{18}O$ (26.9 to 1.7‰) with decreasing Mg and increasing Ca in Ca-poor carbonates (mostly from concretions), and Ca-rich carbonate that dominates ankerite domains and has a large range in chemical composition ($0.4 \leq X_{Ca} \leq 0.7$) with a distribution of $\delta^{18}O$ values indistinguishable from a constant value (5.5 ± 2.2‰), given external precision of our measurements of carbonates. Given textural and chemical differences between these two groups (Figs. 2, 3, and 5), it is plausible that the discontinuity in Figure 7a reflects differences in the conditions of growth or composition of parental fluids between ankeritic domains on one hand and carbonate concretions on the other.

Oxygen isotope compositions of pyroxene, feldspathic glass, and chromite in ALH84001 are simple in comparison to those of carbonate (Fig. 6): Fifty-four measurements of the $\delta^{18}O$ of pyroxene from various crushed and uncrushed portions of the thin section and over a range of distances from carbonate or other phases yield an average and standard deviation of 4.9 ± 1.2‰—homogeneous within analytical precision and within error of the value found by fluorination analyses of bulk materials (Clayton and Mayeda, 1996; Franchi et al., 1997). Feldspathic glass has a $\delta^{18}O$ of 5.0 ± 1.0‰, also homogenous within analytical precision and indistinguishable from the values expected for anorthite-rich melt in equilibrium with pyroxene at magmatic temperatures (≥1000°C; Chiba et al., 1989). Similarly, six analyses of chromite yield an average value of ~2 ± 0.9‰ (these data are not well standardized and the average value should be taken as approximate)—homogeneous within analytical precision and similar to the value of 2.3‰ predicted for equilibrium of Fe-rich spinel with coexisting pyroxene at magmatic temperatures (Chiba et al., 1989). In this context, the contrast between the oxygen isotope geochemistry of carbonate concretions on one hand and ankeritic domains on the other is even more noteworthy. Whereas concretions are isotopically heterogeneous and out of oxygen isotope exchange equilibrium with coexisting phases, Ca-rich carbonates making up the bulk of ankerite domains resemble coexisting silicates and oxides in being isotopically homogeneous and having an average $\delta^{18}O$ that is indistinguishable from the value of ~6.0‰ in equilibrium with coexisting pyroxene, glass, and oxide. Taken at face value, these results suggest that carbonate concretions formed at low temperatures (where oxygen isotope variations are typically large and do not approach local equilibrium) and the Ca-rich carbonate in ankeritic domains might have formed or last equilibrated with coexisting silicate and oxide phases during a high-temperature event, such as brief heating during shock metamorphism, which is believed responsible for the formation of feldspathic glass in this sample (Mittlefehldt, 1994; Treiman, 1995, 1998).

6. TRACE ELEMENTS IN CARBONATE

The abundances of select trace elements (Ba, Sr, Rb, B, Th, U, Zr, Y, La, Ce, and Nd) were measured in 20 spots of carbonate in ALH84001 by secondary ion mass spectrometry using a Cameca ims 4f ion microprobe following techniques described in Veizer et al. (1987) and standardized with natural carbonates. Results of these measurements are presented in Table 5 and plotted in Figure 8 as C1-chondrite–normalized concentrations; data for Mg-rich rims of carbonate concretions are presented in Figure 8a, for cores of carbonate concretions in Figure 8b, and for ankeritic carbonate domains in Figure 8c. To first order, all carbonates in ALH84001 display similar trace-element characteristics: rare earth elements (REE), Y, and Th abundances near or somewhat enriched relative to C1 chondrites, subchondritic B, Rb, and, particularly, Zr abundances, and U, Sr, and Ba concentrations strongly enriched relative to C1 chondrites.

In the following paragraphs, we consider the trace-element compositions of carbonates in ALH84001 from two standpoints: relationships between trace-element and oxygen isotope geochemistry with particular reference to the constraints these relationships might place on the temperatures of carbonate precipitation, and comparison with trace-element abundances in representative terrestrial carbonates of known origin.

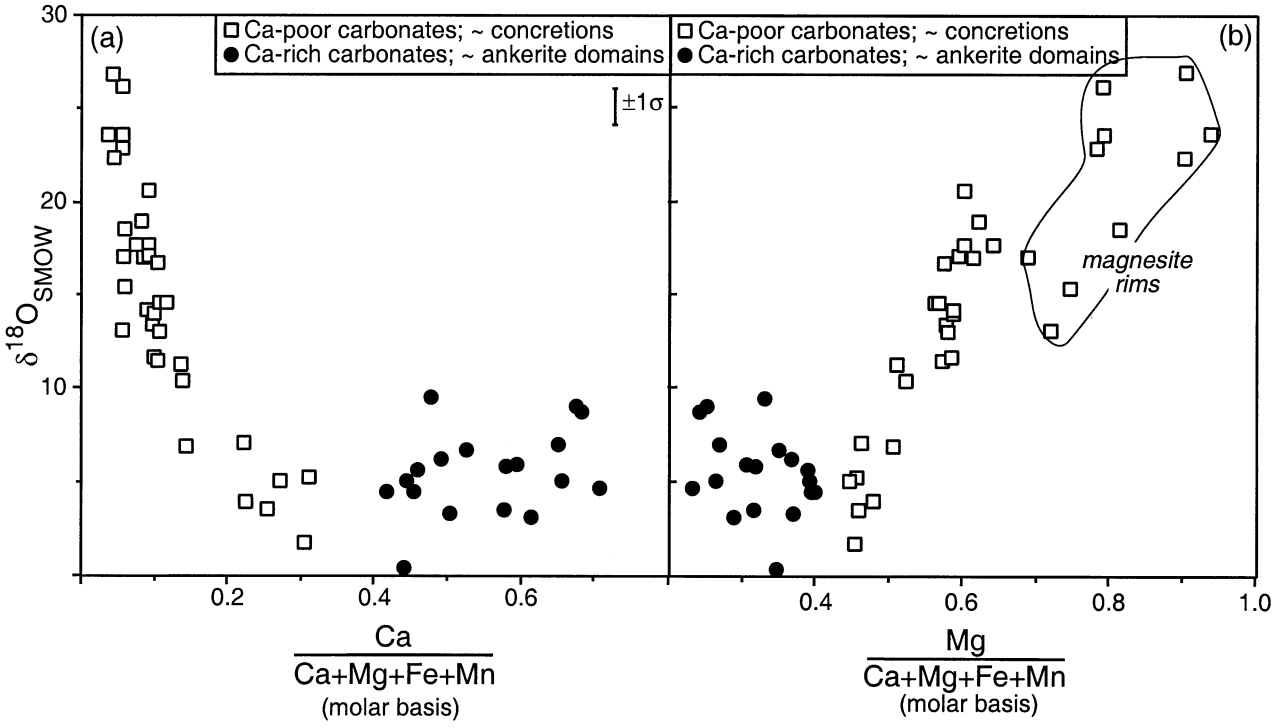

Fig. 7. Oxygen isotope compositions of carbonates in ALH84001.119, plotted as a function of major-element composition determined by electron microprobe. Ca-rich, Mg-poor carbonates from ankerite domains are essentially indistinguishable from one another in $\delta^{18}O$ despite a large range in major element composition, whereas Ca-poor carbonates (mostly from concretions) span a large range in $\delta^{18}O$, correlated with their chemistry. Mg-rich rims of concretions form a distinct population in (b), identified by a dashed field.

6.1. Quantitative Paleo-Thermometry of Carbonate in ALH84001

In the following discussion, we evaluate the possibility that variations in the abundance of trace elements and $\delta^{18}O$ might reflect, entirely or in part, variations in the temperature of carbonate precipitation. We have argued on structural grounds that orange cores of carbonate concretions are metastable precipitates; it follows that a fluid/mineral thermometer based on their compositions must not record equilibrium at the lowest

Table 5. Trace-element analyses of carbonates in ALH84001.

$CaCO_3$ (mole fraction)	Sr (ppm)	Ba (ppm)	La (ppm)	Ce (ppm)	Nd (ppm)	Y (ppm)	B (ppm)	Rb (ppm)	Zr (ppm)	Th (ppm)	U (ppm)
0.04	42.4	5.58	0.67	1.54	1.75	3.32	0.58	0.44	0.71	0.25	0.22
0.05	62.7	11.70	0.21	0.48	0.41	1.70	0.35	1.18	0.99	0.09	0.08
0.05	66.7	6.32	0.41	0.91	0.71	5.63	0.29	0.64	0.12	0.03	0.09
0.06	68.3	8.34	1.31	3.20	2.77	6.47	0.49	0.37	0.97	0.41	0.27
0.07	56.7	6.81	1.64	4.10	3.15	6.93	0.99	0.36	0.92	0.62	0.23
0.08	76.6	10.8	0.87	2.11	1.30	8.43	0.38	1.35	0.44	0.00	0.11
0.09	110	19.9	0.23	0.53	0.63	3.26	0.33	0.37	0.44	0.18	0.13
0.09	84.5	12.1	0.25	0.37	0.81	3.84	0.56	0.35	0.17	0.15	0.15
0.10	92.8	13.5	0.39	0.72	0.76	4.45	0.57	0.71	0.27	0.17	0.24
0.10	110	20.5	0.28	0.49	0.67	3.34	0.60	0.66	0.36	0.21	0.21
0.12	96	26.9	0.25	0.60	0.44	3.22	0.45	0.25	0.15	0.06	0.14
0.14	92.6	27.2	0.27	0.49	0.59	4.87	0.47	0.33	0.22	0.06	0.18
0.15	59.8	31.3	0.59	1.71	1.03	8.56	0.45	0.45	0.33	0.02	0.04
0.22	62.1	80.6	1.34	3.19	2.65	15.2	0.61	0.34	0.29	0.11	0.13
0.23	96.9	78.9	0.98	2.22	1.72	10.2	0.28	2.04	0.20	0.04	0.01
0.25	143	94.5	0.98	2.32	1.34	10.2	0.25	0.74	0.17	0.03	0.04
0.44	357	105	0.91	1.89	1.45	11.4	0.24	0.87	0.22	0.02	0.02
0.45	386	127	1.33	2.69	1.98	13.5	0.29	0.52	0.22	0.03	0.22
0.50	422	151	0.55	0.89	0.97	10.5	0.23	1.68	0.63	0.09	0.25
0.54	453	151	1.52	2.78	2.33	15.2	0.19	0.27	0.18	0.16	0.30

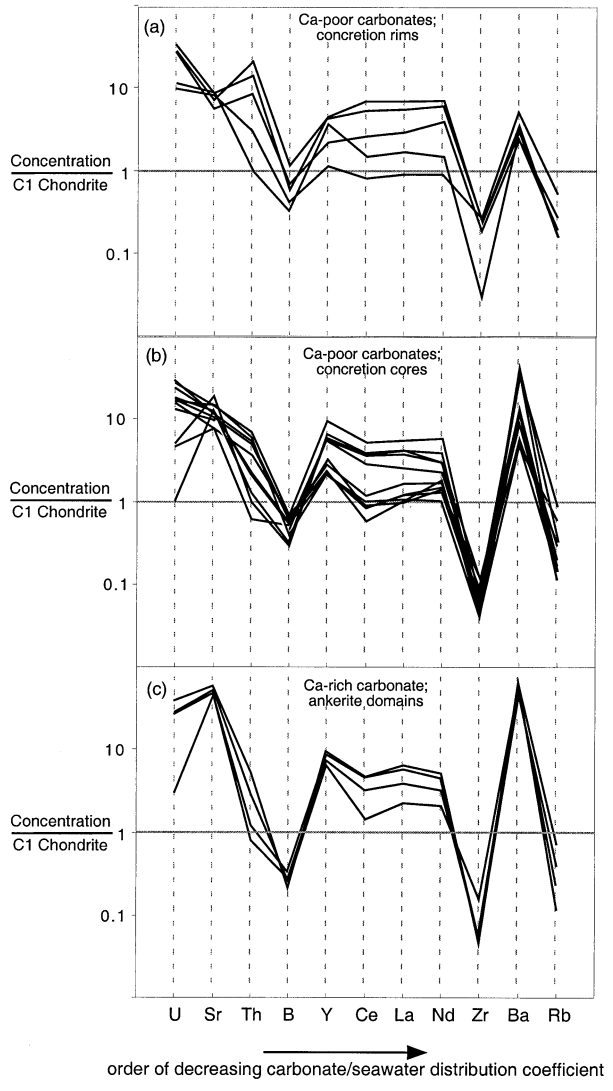

Fig. 8. CI chondrite normalized trace-element abundances in carbonates from ALH84001.119, as determined by ion microprobe. (a) Data for magnesite rims of concretions (Fig. 2). (b) Data for magnesiosiderites from concretion cores (Fig. 2). (c) Data for Ca-rich carbonate from ankerite domains (Fig. 3).

free energy state. This is a significant impediment for precise (i.e., ± 1°C) thermometry in paleoclimatologic studies. However, it is well established that oxygen isotope fractionations between fluids and minerals generally approach within ~0 to 3‰ equilibrium isotopic distributions for a wide diversity of metastable structures and precipitation mechanisms; examples include mollusk shells (Esptein et al., 1953), corals (McConnaughey, 1989), sponges (Bohm et al., 2000), and foraminiferal and diatomaceous tests (e.g., Spero et al., 1997). We conclude on the basis of these past experiences that oxygen isotope compositions of metastable carbonates in ALH84001 could plausibly record their temperatures of precipitation, albeit with systematic offsets that may be as large as several per mil (comparable to the errors of our measurements). Similarly, we note that precise geothermometry based on fluid/mineral partitioning of oxygen isotopes and trace metals depends strongly on solute chemistry, crystal chemistry, kinetic and vital effects and diagenesis (e.g., Koch, 1998). Many of these factors cannot be evaluated with confidence for secondary carbonates in SNC meteorites and therefore we restrict our discussion to a relatively simple question; are variations in the abundances of select trace elements in carbonates from ALH84001 consistent with variations in $\delta^{18}O$ in those carbonates if both reflect only changes in the temperature of carbonate precipitation from a fluid of fixed composition? Although in principle the abundance of several trace elements (e.g., Sr, U, Ba) can serve as tests of this hypothesis, two factors lead us to consider only a comparison of $\delta^{18}O$ variations with Sr/Ca thermometry. First, trace elements other than Sr that are commonly used as thermometers for carbonate precipitation (e.g., U, Ba) are low in abundance in ALH84001 carbonates and therefore their analysis by ion probe is relatively imprecise and more likely to be inaccurate when compared with Sr, which is present at concentrations of hundreds of parts per million. Second, the Sr/Ca thermometer for carbonate precipitation is more established and widely used than other trace-element thermometers and therefore can be evaluated with relative confidence.

Before discussion of the results of our comparison of Sr/Ca ratios with $\delta^{18}O$ values in ALH84001 carbonates, we note a significant property of the combined use of Sr/Ca and $\delta^{18}O$ thermometry. Although both the Sr/Ca or $\Delta^{18}O$ thermometers, when used alone, require knowledge of the composition of both a carbonate mineral and its parental fluid, their simultaneous solution for minerals precipitated from a common solution over a range of temperatures can yield a quantitative temperature estimate without knowledge of either Sr/Ca or $\delta^{18}O$ of the fluid phase. This is because the temperature sensitivity of oxygen isotope fractionations between fluids and carbonates is highly nonlinear at temperatures below ~300° C (O'Neil et al., 1969), whereas the temperature sensitivity of Sr/Ca ratio fractionation between water and carbonate is approximately linear (e.g., Kinsman and Holland, 1969; Devilliers et al., 1994; Shen et al., 1996). As a result, the slope or curvature of any trend in a plot of $\delta^{18}O$ vs. Sr/Ca ratio for a population of carbonates grown from a common fluid can be consistent with the equilibrium relationship only over a specific range of temperatures. Finally, we reiterate that textural, major element and oxygen isotope evidence suggests that ankeritic domains may be different in origin from carbonate concretions. Therefore, we apply this test only to carbonate concretions (which record a wide range in $\delta^{18}O$ and Sr/Ca ratio) and show data for ankeritic domains (which do not) only for comparison.

Figure 9 illustrates the combined application of oxygen-isotope and Sr/Ca thermometry to carbonates in ALH84001. It was not possible using our techniques to directly measure $\delta^{18}O$ and trace-element composition on the same volume of carbonate (i.e., closely adjacent points or even serial measurements of the same hole may not sample the same composition material). Therefore we compare $\delta^{18}O$ with Sr/Ca by combining known relationships between $\delta^{18}O$ and Ca content (Fig. 9a) and between Sr/Ca ratio and Ca content (Fig. 9b); in both cases three-point floating averages of the data were calculated and the Sr/Ca ratio compared with $\delta^{18}O$ values for any given Ca content based on polynomial regression of the resulting trends. The results are plotted in Figure 9c, which shows the molar Sr/Ca ratio on the left vertical axis vs. the $\delta^{18}O_{SMOW}$ value on

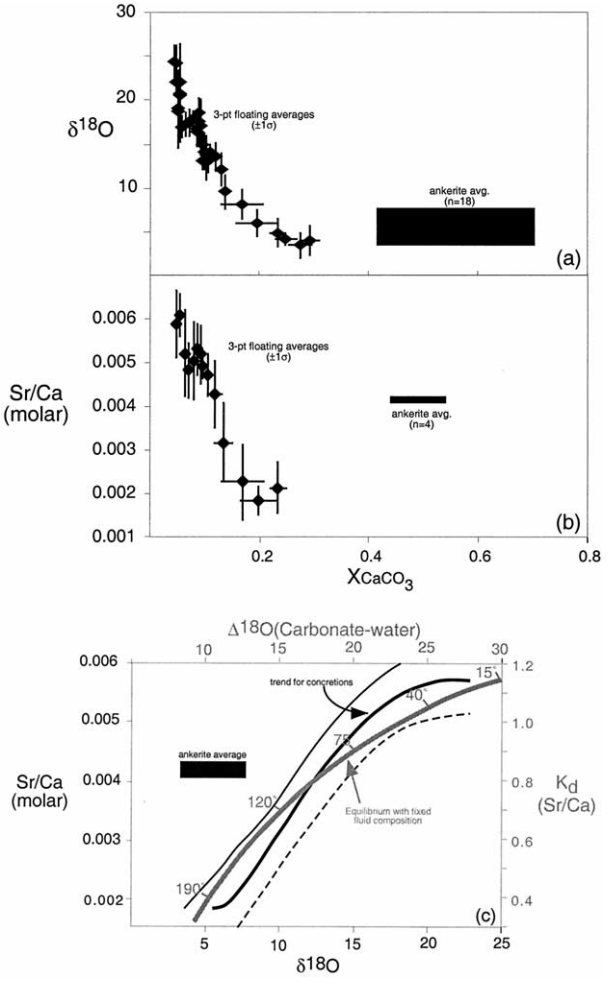

Fig. 9. Comparison of carbonate $\delta^{18}O$-Sr/Ca systematics with those expected for polythermal precipitation from a fluid of constant composition. (a) Three-point floating average for the trend of $\delta^{18}O$ vs. X_{CaCO_3} measured in ALH84001 carbonates (see Fig. 7a). Error bars show $\pm 1\sigma$ variation about these averages. Ca-rich carbonates are indistinguishable from a single $\delta^{18}O$ and are shown as a box having vertical dimension of $\pm 1\sigma$ for measured values and horizontal dimension of the measured range in X_{CaCO_3}. (b) Three-point floating average for the trend of Sr/Ca ratio vs. X_{CaCO_3} measured in ALH84001 carbonates. Error bars show $\pm 1\sigma$ variation abot these averages. Ca-rich carbonates are indistinguishable from a single Sr/Ca ratio and are shown as a box having vertical dimension of $\pm 1\sigma$ for measured values and horizontal dimension of the measured range in X_{CaCO_3}. (c) Plot of Sr/Ca ratio vs. $\delta^{18}O$ measured for magnesio-siderite concretions (black curve) and ankerite domains (black square). The black curve is based on polynomial fits to data for concretions presented in (a) and (b) so that Sr/Ca and $\delta^{18}O$ values of carbonates having a given Ca content can be estimated (dashed curves are $\pm 1\sigma$ envelope). The black field is the average and $\pm 1\sigma$ range for ankeritic carbonate. These data use the left-hand vertical scale and bottom horizontal scale. The gray curve is the estimated equilibrium relationship between $\Delta^{18}O$ (carbonate–water) and Kd (Sr/Ca) for carbonate/water over a range in temperatures (based on data from O'Neil et al., 1969, and Kinsman and Holland, 1969). These data use the right-hand vertical scale and the top horizontal scale. The correlation between $\delta^{18}O$ and Sr/Ca in carbonate concretions from ALH84001 is consistent with precipitation from a single water having $\delta^{18}O$ of about $-5‰$ and Sr/Ca ratio of ~0.005 between temperatures of ~190°C (for Fe- and Ca-rich concretion cores) and ~20°C (for Mg-rich concretion rims). Ankeritic carbonate does not fall on this trend; in the context of these model calculations, ankerite cannot be precipitated at any temperature from the same fluid that is parental to concretions.

the bottom horizontal axis. The solid black curve is our estimated relationship between $\delta^{18}O$ and Sr/Ca based on data in Figures 9a,b; dashed black curves are $\pm 1\sigma$ error envelopes to this relationship. We have overlain onto this plot the equilibrium relationship of $\Delta^{18}O_{water\text{-}carbonate}$ (top horizontal axis) vs. the value of K_d(Sr/Ca) —i.e., $[Sr/Ca]_{carbonate}/[Sr/Ca]_{water}$ (right vertical axis) at temperatures of 15 to 200°C. The estimated equilibrium relationship is based on data from Kinsman and Holland (1969) and O'Neil et al. (1969); these experiments do not differ significantly from more recent constraints from studies of natural systems (e.g., Devilliers et al., 1994; Shen et al., 1996) given the large range of compositions we wish to interpret and the uncertainties of our data. The scales of top and bottom horizontal axes have the same range in units of $\delta^{18}O$ and the left and right vertical axes have the same proportional range in the Sr/Ca ratio (i.e., the scale for the equilibrium relationship is equal to the scale for the data).

The observations for carbonate concretions are consistent with the equilibrium trend over a temperature interval of ~20 to 190°C, both in terms of relative ranges in both $\delta^{18}O$ and Sr/Ca ratio and in the curvature of the relationship between these two variables. The curvature in the data trend prohibits fitting the data to the equilibrium curve at significantly higher or lower temperatures, where the equilibrium relationship is relatively straight and has a slope consistent with only a portion of the trend of data. We conclude that covariation of Sr/Ca ratios and $\delta^{18}O$ in carbonate concretions in ALH84001 supports the hypothesis that they precipitated from an aqueous solution of broadly constant $\delta^{18}O$ and Sr/Ca ratio over a range in temperatures approximating the low pressure stability limits of liquid water. To our knowledge, the only experiment to successfully precipitate carbonate concretions with the distinctive chemical zonation of those in ALH84001 did so at temperatures of 25 and 150°C in a closed system (Golden et al., 2001).

Before exploring the implications of this result more thoroughly, we note a clear caveat: we have demonstrated that trace-element and oxygen isotope compositions are *consistent* with polythermal precipitation from a low-temperature aqueous fluid, but do not require it. In particular, it is possible that systematic variations in solution chemistry (including both Sr/Ca ratio and $\delta^{18}O$) at a fixed temperature could produce the trend observed in Figure 9c. This alternative hypothesis is somewhat arbitrary and seems unlikely given the specific requirements of coupled Sr/Ca ratio and $\delta^{18}O$ changes needed to mimic the equilibrium trend. However, to our knowledge, it cannot be disproved.

6.2. Chemistry of Fluids Parental to Carbonate

Results described in the preceding sections indicate that carbonate concretions in ALH84001 could have grown over a range in temperatures of ~20 to 190°C from fluids of approximately constant Sr/Ca ratio and $\delta^{18}O$. A logical extension of this conclusion is that the values of $\delta^{18}O$ and trace-element compositions measured in this study can be interpreted as quantitative constraints on the composition of the parental fluid.

Estimating the $\delta^{18}O$ of fluid parental to carbonates in ALH84001 (assuming consistency with the hypothesis described above) is relatively straightforward. Comparison of the

top and bottom axes of Figure 9c indicates that carbonates having $\delta^{18}O$ values between ~5 and 25‰ grew at temperatures such that the carbonate–water fractionation was 10 to 30‰, and thus the $\delta^{18}O$ of parental fluid is −5‰ (neglecting the subtle nonlinearity in the $\delta^{18}O$ scale). This value is significantly ^{18}O depleted relative to terrestrial seawater (0‰), terrestrial magmatic waters (6 to 10‰), and the expected composition of martian magmatic waters (estimated 5 to 10‰). Therefore our results suggest that carbonates in ALH84001 precipitated from a near-surface reservoir of water that is mass-fractionated in its isotopic composition relative to primordial Marian volatiles. We suggest three plausible mechanisms for generating such a reservoir.

(1) Low-temperature water–rock interaction in the martian crust, which is expected to generate high-$\delta^{18}O$ alteration phases and low-$\delta^{18}O$ residual waters. The presence of high-$\delta^{18}O$ (~15 to 30‰) alteration minerals in ALH84001, Nakhla, and Lafayette indicates that such processes have taken place. Note that analogous processes would be expected to make the Earth's ocean similarly low in $\delta^{18}O$ (estimated −10 to −20‰) in the absence of high-temperature water–rock interaction in midocean-ridge hydrothermal systems (Gregory, 1991); therefore, near-surface waters in a planet lacking active submarine ridges should have a relatively low-$\delta^{18}O$ hydrosphere.
(2) Exchange of oxygen isotopes between liquid water and atmospheric CO_2 near the martian surface (see Clayton and Mayeda, 1988). It is difficult to predict the strength of ^{18}O depletion that could be caused by such a process because the $\delta^{18}O$ of the martian atmosphere is not well known. However, given the expected $\delta^{18}O$ of martian magmatic volatiles, the size of the water-CO_2 fractionation at 0°C, and the possibility that CO_2 in the martian atmosphere is itself mass fractionated as a result of cycles of condensation and sublimation of CO_2 ice (Eiler et al., 2000), a value of −5‰ is possible.
(3) Cycles of melting, freezing, evaporation, sublimation, and condensation of water in the martian near-surface environment are expected to produce mass-fractionated reservoirs of water by processes similar to those responsible for ^{18}O depletion in terrestrial meteoric water relative to the terrestrial ocean. In particular, martian waters that are residual to growth of water ice could have ^{18}O depletions of this magnitude, as could martian waters formed directly or indirectly by precipitation from an atmospheric water reservoir.

Estimating the trace-element composition of fluids parental to carbonates in ALH84001 is less certain because many factors influence elemental partitioning between carbonates and aqueous fluids (some of which were referred to in the preceding section). Given uncertainties about these factors and the precision of ion microprobe measurements, we think it is more straightforward to simply compare broad features of the trace-element abundances in carbonates from ALH84001 to those in representative terrestrial carbonates of known origin (Fig. 10). This comparison reveals that, to first order, the abundances of trace elements in carbonates in ALH84001 are most similar to those in terrestrial marine carbonates—that is, both are characterized by relatively high U, Th, and Sr abundances, relatively low Rb and Zr abundances, and near-chondritic abundances of REEs. Trace-element abundances in ALH84001 carbonates are relatively unlike those of terrestrial carbonatites (which have exponentially higher overall trace-element abundances and near-chondritic interelement ratios involving Sr, REEs, and Zr) and hydrothermal carbonates (which are characterized by far higher REE abundances, strong negative Y anomalies, and near-chondritic ratios of Sr to REEs). However, terrestrial marine carbonates are characterized by higher abundances of B and Zr and lower abundances of Ba compared with ALH84001 carbonates. These differences could reflect any of a number of factors. For example, low Ba abundances in terrestrial marine carbonates reflect scavenging of Ba from seawater by barite; thus, higher Ba contents of carbonates in ALH84001 could indicate that they precipitated from an aqueous solution broadly similar to seawater but unaffected by precipitation of barite. Similarly, we infer that ALH84001 carbonates precipitated at somewhat higher temperatures than current Earth surface conditions, such that the strong negative Zr anomaly most characteristic of hydrothermal carbonates that grow near fluid–mineral equilibrium would develop. We conclude that although the exact causes of some interelement ratios can only be guessed at, the minor element chemistry of carbonates in ALH84001 plausibly reflects precipitation from solutions having concentrations of lanthanides, actinides, alkalis, and Sr broadly similar to those in terrestrial seawater. This conclusion, combined with the preceding discussion of the temperatures of

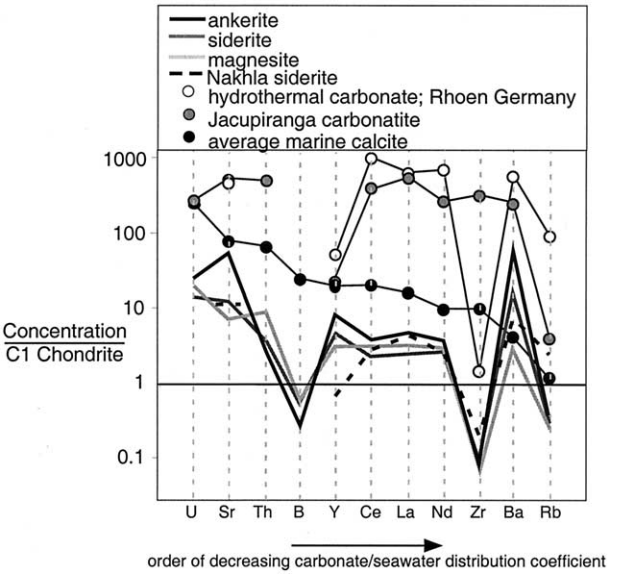

Fig. 10. Comparison of average, CI-normalized trace-element compositions of ALH84001 carbonates (heavy lines) to those for representative terrestrial carbonates (circles joined by light lines) including marine calcite (black circles), carbonatite (gray circles), and hydrothermally altered carbonate (open circles); data are ordered from left to right by increasing compatibility in marine carbonate compared with seawater. ALH84001 carbonates are broadly similar to marine calcite in overall pattern (i.e., U and Sr are more abundant than Y or REE; low overall concentrations), but have relatively low Zr and B abundances and relatively high Ba abundances. Data for Nakhla siderite from Wadhwa and Croaz (1998) are shown for comparison as a heavy dashed line. Data for terrestrial carbonates are taken from Huang et al. (1995), Utzmann et al. (1999), and Veizer (1983).

carbonate precipitation, suggests that at the time of aqueous alteration of ALH84001, Mars contained at least local reservoirs of low-temperature crustal or surface waters whose cation chemistry resembles seawater. These constraints are consistent with either evaporitic or low-temperature diagenetic environments for precipitation of carbonate concretions and inconsistent with models involving carbonate concretion formation by high-temperature hydrothermal alteration, metamorphism, or carbonate-melt injection.

7. ORIGIN OF ANKERITIC DOMAINS

An important result of our geochemical and textural studies is the identification of differences in major-element and oxygen isotope composition and texture between carbonate concretions on one hand and ankeritic domains on the other. Preceding sections describing the structural properties, temperatures of origin, and chemistry of parental solutions apply only to the first of these carbonate types and place no obvious constraints on the origins of the second. In this section, we consider the implications of our observations for the origin of ankeritic domains and the relationship of those domains to carbonate concretions. The following summarizes the key arguments on the origin of ankeritic carbonate domains.

(1) The geochemical arguments in favor of a low-temperature origin of carbonate concretions (oxygen isotope variability and disequilibrium with coexisting phases; complex, fine-scale cation zonation; major-element compositions in violation of the ankerite/magnesio-siderite solvus) do not apply to Ca-rich carbonate making up most of ankerite domains.
(2) Major element compositions of some Ca-rich carbonates fall inside the calcite–ankerite solvus at 300 to 700°C and could be metastably precipitated. However, the calcite–ankerite solvus closes at higher temperatures, unlike the ankerite–magnesio-siderite solvus, and thus these Ca-rich carbonates, could form under equilibrium conditions at magmatic temperatures.
(3) Feldspathic glass does not appear to cross-cut preexisting internal structures of ankerite domains as it does those of carbonate concretions; instead, it is present as abundant, intimately intergrown blebs or beads.
(4) Pyroxene surrounds and encloses ankerite domains (as with other carbonate populations in ALH84001) but is also present as abundant, disseminated, and equant grains entirely enclosed by carbonate.
(5) Relative abundances of trace elements in ankerite domains are broadly similar to those in other ALH84001 carbonates.
(6) Contacts between ankerite domains and pyroxenes generally lack magnesite rims typical of concretions.
(7) Ankerite domains are approximately in high-temperature oxygen isotope exchange equilibrium with coexisting pyroxene and feldspathic glass (at least insofar as their $^{18}O/^{16}O$ ratios are concerned; i.e., ^{17}O has not been measured in ankerite domains as distinct from other carbonates).
(8) Ca-rich carbonate from ankerite domains is nearly constant in Fe/Mg and Mn/Ca ratios, but are distinct in Ca-Mg-Fe-Mn composition from concretions.

Collectively, these observations suggest that there is no compelling reason to believe ankerite domains are generated by the same low-temperature aqueous precipitation processes called upon by this and previous studies to explain the presence of carbonate concretions. We believe these domains are better described by a high-temperature origin. In particular, the textures illustrated in Figure 3, homogeneity and equilibrium with coexisting phases characteristic of their oxygen-isotope compositions, and their simple variations in cation chemistry (i.e., fixed Fe/Mg and Mn/Ca ratios) might be explained by formation from a carbonate-rich shock melt that phase-separated into ankerite and feldspathic glass on quenching. This suggestion follows the models of Scott et al. (1997, 1998), although they applied that model to all carbonates in ALH84001, whereas we suggest that it is appropriate for ankerite domains but is not consistent with the properties of concretions. This hypothesis explains the unusual textural relationship between ankerite domains and pyroxene (i.e., the presence of finely disseminated pyroxene crystals and clots within ankerite) because it is reasonable to suppose that approximately millimeter-scale bodies of shock melt might entrain fragments of surrounding shock-breciated host rock while still in a fluid state. In the context of this model, the similarities in trace-element composition between concretions and ankerite domains suggest that the carbonate fraction of these shock melts is derived from shock melting of preexisting concretions. Scott et al. (1998) suggest that carbonate in ALH84001 was produced by shock melting of preexisting aqueous precipitates; where our suggestion differs is that we believe both shock melts and their progenitor low-temperature precipitates are present in the rock. Ankerite domains are the former, whereas more abundant concretions are the latter. In this sense, one could view ankerite domains and associated feldspathic glass as an extreme product of the same process by which partially decomposed carbonate fragments became entrained in feldspathic glass elsewhere in this sample (McKay et al., 1997). Finally, this interpretation suggests that ankeritic domains are younger than concretions because feldspathic glass (by this view syngenetic with ankerite domains) cross-cut concretions (Fig. 2; McKay et al., 1997). Unfortunately, we do not believe the section we have examined preserves a clear cross-cutting relationship between carbonate concretions and ankeritic domains; search for such a textural relationship is an important goal for future work.

The major-element compositions of ankerite domains offer tests of the hypothesis that they underwent high-temperature exchange with coexisting silicates. For example, our previous discussion of the oxygen isotope geochemistry of ALH84001 suggests that ankerite should approach Fe/Mg exchange equilibrium with coexisting orthopyroxene. Molar Fe/Mg ratios in orthopyroxene from ALH84001 are 0.38—indistinguishable from the value of ~0.4 characteristic of Ca-rich carbonate from ankerite domains (i.e., K_d for Fe/Mg distribution between ankerite and orthopyroxene is ~1). Experimental studies of the carbonate–olivine and carbonate–olivine–pyroxene system shows that at high temperatures (~1000°C) and pressures (15 to 25 kbar) the distribution coefficient $(Fe/Mg)_{carbonate}/(Fe/Mg)_{silicate}$ for ankerites containing more than 50 mol% $CaCO_3$ is equal to 1 (Dalton and Wood, 1993); therefore, the Fe/Mg ratio characteristic of ankerite domains plausibly reflects high-temperature exchange with coexisting silicates. Similarly, ankerites and carbonate melts in equilibrium with ultramafic

mineralogies and/or anorthite-rich melts at high temperatures and pressures are characterized by Ca contents intermediate between calcite and ankerite solid solutions—like Ca-rich carbonate in ankerite domains from ALH84001 (e.g., Dalton and Wood, 1993; Lee and Wyllie, 1997).

It is important to note that the stability of carbonate–silicate assemblages at high temperature restricts the pressures at which Fe/Mg exchange must have taken place according to this hypothesis. Pressures of at least 15 to 20 kbar are required to prevent decarbonation reactions in assemblages of magnesian calcite and ultramafic silicates (Dalton and Wood, 1993). We can imagine no scenarios in which such pressures could have been reached in ALH84001 other than during a transient shock metamorphic event. It is not obvious to us whether systems of the type we consider can closely approach Fe/Mg and oxygen isotope equilibrium during the short times of shock pressurization and heating; we suggest that this question is an attractive target for future experimental work.

8. SUMMARY AND CONCLUSIONS

Textural and geochemical data presented here document the existence of two distinct populations of carbonate in ALH84001. One of these is composed of carbonate concretions whose chemical and structural properties suggest they are low-temperature aqueous precipitates; the other is texturally and geochemically distinct from concretions, concretion fragments, or partial (e.g., edge-on) samples of concretions and has geochemical properties suggesting that it formed by processes and under conditions different from those of concretion precipitation. Several previous studies of ALH84001 have deduced the properties of its carbonates on the basis of bulk-rock properties; ages and $\Delta^{17}O$ values of carbonates in particular are based on acid etches of whole-rock samples and do not discriminate between carbonates of different textural type (Farquhar et al., 1998; Borg et al., 1999). Our results suggest that these measurements may reflect physical mixing in unknown proportions of analyte extracted from concretions on one hand and ankerite domains on the other.

Coupled major-element, trace-element, and oxygen isotope systematics in carbonate concretions from ALH84001 define trends that constrain the conditions of carbonate precipitation and the nature of the parental fluid. Among the trends defined by these data is a correlation between $\delta^{18}O$ and Sr/Ca ratio, which could have several possible interpretations but is notably similar to that one would predict for precipitation of carbonate from a solution of fixed Sr/Ca ratio and $\delta^{18}O$ over a range in temperature from ~20 to 190°C. To our knowledge, this is the only temperature estimate for carbonate formation in ALH84001 that is based only on principles of cation and oxygen isotope exchange thermometry and not on model assumptions of the origin of fluids parental to carbonate (other than that this fluid is constant in $\delta^{18}O$ and Sr/Ca ratio). Carbonate precipitation experiments indicate that concretions resembling those in ALH84001 can be formed by precipitation from a reservoir of fluid at temperatures within this range (Golden et al., 2000); however, further work will be needed to determine whether the thermal history we suggest and some of the other details of ALH84001 carbonate chemistry (e.g., zonation in Mn content) can be experimentally reproduced.

Finally, our results document a consistent pattern to the relative abundances of trace elements in ALH84001 carbonates and their comparison with relative abundances of those elements in terrestrial carbonates. Although these elemental abundance ratios vary in detail (e.g., Sr/Ca varies by a factor of four; Fig. 9), their overall patterns are much like those of terrestrial marine calcites and unlike those of many terrestrial hydrothermal and magmatic carbonates. This result, when combined with other conclusions of this study, suggests that carbonate concretions precipitated from a low-temperature aqueous solution broadly similar in minor-element composition to terrestrial seawater and remobilization of this carbonate by shock processes can explain the compositions of carbonates with massive textures, simpler cation variations and oxygen-isotope equilibrium with coexisting silicates.

Acknowledgments—This research was supported by NSF, DOE, and NERC. We thank Ronit Kessel for her helpful comments on an early draft of the manuscript. We thank Ed Scott and David Mittlefehldt for thorough and helpful reviews and Horton Newsom for editorial handling of the manuscript. We also thank John Craven for his support in use of the University of Edinburgh ion microprobe laboratory, Richard Hinton for his advice on trace-element analyses, and George Rossman for his assistance and advice with FTIR and X-ray diffraction analyses.

Associate editor: H. E. Newsom

REFERENCES

Adler H. H. and Kerr P. F. (1963) Infrared adsorption frequency trends for anhydrous normal carbonates. *Am. Mineral.* **48,** 124–137.

Bader R. G. et al., Initial Reports of the Deep Sea Drilling Program (1970) Vol. IV. National Science Foundation, Washington (US Government Printing Office). 753 pp.

Bohm F., Joachimski M. M., Dullo W. C., Eisenhauer A., Lahnert H., Reitner J., and Worheide G. (2000) Oxygen isotope fractionation in marine aragonite of coralline sponges. *Geochim. Cosmochim. Acta* **64,** 1695–1703.

Borg L. E., Connelly J. N., Nyquist L. E., Shih C. Y., Wiesmann H., and Reese Y. (1999) The age of the carbonates in martian meteorite ALH84001. *Science* **286,** 90–94.

Bradley J. P., Harvey R. P., and McSween H. Y. (1996) Magnetite whiskers and platelets in the ALH84001 martian meteorite: Evidence of vapor phase growth. *Geochim. Cosmochim. Acta* **60,** 5149–5155.

Carr R. H., Grady M. M., Wright I. P., and Pillinger C. T. (1985) Martian atmospheric carbon dioxide and weathering products in SNC meteorites. *Nature* **314,** 248–250.

Chiba H., Chacko T., Clayton R. N., and Goldsmith J. R. (1989) Oxygen isotope fractionations involving diopside, forsterite, magnetite and calcite: Application to geothermometry. *Geochim. Cosmochim. Acta* **53,** 2985–2995.

Clayton R. N. and Mayeda T. K. (1988) Isotopic composition of carbonate in EETA 79001 and its relation to parent body volatiles. *Geochim. Cosmochim. Acta* **52,** 925–927.

Clayton R. N. and Mayeda T. K. (1996) Oxygen isotope studies of achondrites. *Geochim. Cosmochim. Acta* **60,** 1999–2017.

Cooney T. F., Scott E. R. D., Krot A. N., Sharma S. K., and Yamaguchi A. (1999) Vibrational spectroscopic study of minerals in the Martian meteorite ALH84001. *Am. Mineral.* **84,** 1569–1576.

Curtis C. D., Coleman M. L., and Love L. G. (1986) Pore water evolution during sediment burial from isotopic and mineral chemistry of calcite, dolomite and siderite concretions. *Geochim. Cosmochim. Acta* **50,** 2321–2334.

Dalton J. A. and Wood B. J. (1993) The partitioning of Fe and Mg between olivine and carbonate and the stability of carbonate under mantle conditions. *Contrib. Mineral. Petrol.* **114,** 501–509.

Davidson P. M. (1994) Ternary iron, magnesium, calcium carbonates: A thermodynamic model for dolomite as an ordered derivative of calcite-structure solutions. *Am. Mineral.* **79,** 332–339.

Deelman J. C. (1999) Low-temperature nucleation of magnesite and dolomite. *Neues Jahrbuch Mineral. Monatshefte* **7,** 289–302.

Devilliers S., Shen G. T., and Nelson B. K. (1994) The Sr/Ca-temperature relationship in coralline aragonite—Influence of variability in $(Sr/Ca)_{seawater}$ and skeletal growth parameters. *Geochim. Cosmochim. Acta* **58,** 197–208.

Dubrawski J. V. and Channon A.-L. (1989) Examination of the siderite-magnesite mineral series by Fourier transform infrared spectroscopy. *Am. Mineral.* **74,** 187–190.

Dubrawski J. V., Channon A. L., and Warne S. St. J. (1989) The effects of substitution in the dolomite–ferroan dolomite–ankerite series as illustrated by FTIR. *Neues Jahrbuch Mineral. Monatshefte* **8,** 337–344.

Eiler J. M., Graham C. M., and Valley J. W. (1997a) SIMS analysis of oxygen isotopes: Matrix effects in complex minerals and glasses. *Chem. Geol.* **138,** 221–244.

Eiler J. M., Graham C. M., and Valley J. W. (1997b) Standardization of SIMS analysis of O and C isotope ratios in carbonates from ALH84001 [abstract]. Presented at the 28th Lunar and Planetary Science Conference.

Eiler J. M., Rahn T., and Kitchen N. (2000) Experimental constraints on the stable isotope systematics of CO_2 ice/vapor systems and relevance to the study of Mars. *Geochim. Cosmochim. Acta* **64,** 733–746.

Epstein S., Buchsbaum R., Lowenstam H. A., and Urey H. C. (1953) Revised carbonate water isotopic temperature scale. *Geol. Soc. Am. Bull.* **64,** 1315–1326.

Essene E. J. (1983) Solid solutions and solvi among metamorphic carbonates with applications to geologic thermobarometry. In *Carbonates: Mineralogy and Chemistry* (ed. R. J. Reeder), Vol. 11, pp. 77–96. Mineralogical Society of America.

Farmer V. C. and Warne S. S. J. (1978) Infrared spectroscopic evaluation of iron contents and excess calcium in minerals of the dolomite-ankerite series. *Am. Mineral.* **63,** 779–781.

Farquhar J., Thiemens M. H., and Jackson T. (1998) Atmosphere-surface interactions on Mars: $\Delta^{17}O$ measurements of carbonate from ALH84001. *Science* **280,** 1580–1582.

Fisler D. K. and Cygan R. T. (1998) Cation diffusion in calcite: Determining closure temperatures and the thermal history for the Allan Hills 84001 meteorite. *Meteor. Planet. Sci.* **33,** 785–789.

Franchi I. A., Sexton A. S., Wright I. P., and Pillinger C. T. (1997) A refinement of oxygen isotopic composition of Mars. *Proc. Lunar Planet. Sci. Conf.* **28,** 379–380.

Gil P. P., Pesquera A., and Valasco F. (1992) X-ray diffraction, infrared and Mossbauer studies of Fe-rich carbonates. *Eur. J. Mineral.* **4,** 521–526.

Golden D. C., Ming D. W., Schwandt C. S., Lauer H. V. Jr., Socki R. A., Morris R. V., Lofgren G. E., and McKay G. A. (2001) A simple inorganic process for formation of carbonates, magnetite, and sulfides in martian meteorite ALH 84001. *Am. Mineral.* **86,** 370–375.

Goldsmith J. R. (1960) Exsolution of dolomite from calcite. *J. Geol.* **68,** 103–109.

Gooding J. L., Wentworth S. J., and Zolensky M. E. (1991) Aqueous alteration of the Nakhla meteorite. *Meteoritics* **26,** 135–143.

Gregory R. T. (1991) Oxygen isotope history of seawater revisited: Timescales for boundary event changes in the oxygen isotope composition of seawater. In *Stable Isotope Geochemistry: A Tribute to Samuel Epstein* (eds. H. P. Taylor, J. R. O'Neil, and I. R. Kaplan), pp. 65–76. Special Publication 3. Geochemical Society.

Harvey R. P. and McSween H. Y. (1996) A possible high-temperature origin for the carbonates in the martian meteorite ALH84001. *Nature* **382,** 49–51.

Huang Y. M., Hawkesworth C. J., Vancalstern P., and McDermott F. (1995) Geochemical characteristics and origin of the Jacupiranga carbonatites, Brazil. *Chem. Geol.* **119,** 79–99.

Kinsman D. J. J. and Holland H. D. (1969) The co-precipitation of cations with $CaCO_3$—IV. The co-precipitation of Sr^{2+} with aragonite between 16° and 96°C. *Geochim. Cosmochim. Acta* **33,** 1–17.

Koch P. L. (1998) Isotopic reconstruction of past continental environments. *Ann. Rev. Earth Planet. Sci.* **26,** 573–613.

Laverne C. (1993) Occurrence of siderite and ankerite in young basalts from the Galapagos spreading center (DSDP Holes 506G and 507B). *Chem. Geol.* **106,** 27–46.

Lee W.-J. and Wyllie P. J. (1997) Liquid immiscibility between nephelinite and carbonatite from 1.0 to 2.5 GPa compared with mantle melt compositions. *Contrib. Mineral. Petrol.* **127,** 1–16.

Leshin L., McKeegan K., and Harvey R. (1998) Oxygen isotopic constraints on the genesis of carbonates from martian meteorite ALH84001. *Geochim. Cosmochim. Acta* **62,** 3–13.

McConnaughey T. (1989) ^{13}C and ^{18}O isotopic disequilibrium in biological carbonates: 2. In vitro simulation of kinetic isotope effects. *Geochim. Cosmochim. Acta* **53,** 163–171.

McKay D. S., Gibson E. K., Thomas-Keprta K. L., Vali H., Romanek C. S., Clemett S. J., Chillier X. D. F., Maechling C. R., and Zare R. N. (1996) Search for past life on Mars: Possible relic biogenic activity in martian meteorite ALH84001. *Science* **273,** 924–930.

McKay G. A., Mikouchi T., and Lofgren G. E. (1997) Carbonates and feldspathic glass in Allan Hills 84001: Additional complications. *Meteor. Planet. Sci.* **32,** A87–A88.

McSween H. Y. (1985) SNC Meteorites: Clues to martian petrologic evolution? *Rev. Geophys.* **23,** 391–416.

McSween H. Y. (1994) What have we learned about Mars from SNC meteorites? *Meteoritics* **29,** 757–779.

McSween H. Y. and Harvey R. P. (1998) An evaporation model for formation of carbonates in the ALH84001 Martian meteorite. *Int. Geol. Rev.* **40,** 774–783.

McSwiggen P. L. (1993) Alternative solution model for the ternary carbonate system $CaCO_3$-$MgCO_3$-$FeCO_3$. 2. Calibration of a combined ordering model and mixing model. *Phys. Chem. Minerals* **20,** 42–55.

Mittlefehldt D. (1994) ALH84001, a cumulate orthopyroxenite of the martian meteorite clan. *Meteoritics* **29,** 214–221.

Mozley P. S. and Carothers W. W. (1991) Elemental and isotopic composition of siderite in the Kuparuk formation, Alaska: Effect of microbial activity and water/sediment interaction on early pore-water chemistry. *J. Sediment. Petrol.* **62,** 681–692.

Nyquist L. E., Bansal B. M., Wiesmann H., and Shih C. Y. (1995) "Martians" young and old: Zagami and ALH84001. *Proc. Lunar Planet. Sci. Conf.* **26,** 1065–1066.

O'Neil J. R., Clayton R. N., and Mayeda T. K. (1969) Oxygen isotope fractionation in divalent metal carbonates. *J. Chem. Phys.* **51,** 5547–5558.

Pouchou J. L. and Pichoir F. (1984) Quantitative microanalytic possibilities using a new formulation of matrix effects. *J. Phys.* **45,** 17–20.

Reeder R. J. (1983) Crystal chemistry of the rhombohedral carbonates. In *Carbonates: Mineralogy and Chemistry* (ed. R. J. Reeder), Vol. 11, pp. 1–48.Mineralogical Society of America.

Romanek C. S., Grady M. M., Wright I. P., Mittlefehldt D. W., Socki R. A., Pillinger C. T., and Gibson E. K. (1994) Record of fluid–rock interactions on Mars from the meteorite ALH84001. *Nature* **372,** 655–657.

Saxton J. M., Lyon I. C., and Turner G. (1998) Correlated chemical and isotopic zoning in carbonates in the martian meteorite ALH84001. *Earth Planet. Sci. Lett.* **160,** 811–822.

Scott E. R. D. (1999) Origin of carbonate-magnetite-sulfide assemblages in Martian meteorite ALH84001. *J. Geophys. Res.* **104,** 3803–3813.

Scott E. R. D., Yamaguchi A., and Krot A. N. (1997) Petrological evidence for shock melting of carbonates in the martian meteorite ALH84001. *Nature* **387,** 377–379.

Scott E. R. D., Krot A. N., and Yamaguchi A. (1998) Formation of preimpact, interstitial carbonates in the Allan Hills 84001 Martian meteorite. *Meteor. Planet. Sci.* **33,** A139–A140.

Shearer C. K., Layne G. D., Papike J. J., and Spilde M. N. (1996) Sulfur isotopic systematics in alteration assemblages in martian meteorite Allan Hills 84001. *Geochim. Cosmochim. Acta* **60,** 2921–2926.

Shen C. C., Lee T., Chen C. Y., Wang C. H., Dai C. F., and Li L. A. (1996) The calibration of D[Sr/Ca] versus sea surface temperature relationship for Porites corals. *Geochim. Cosmochim. Acta* **60,** 3849–3858.

Spero H. J., Bijma J., Lea D. W., and Bemis B. E. (1997) Effect of seawater carbonate concentration on foraminiferal carbon and oxygen isotopes. *Nature* **390,** 497–500.

Stranger G. and Neal C. (1994) The occurrence and chemistry of huntite from Oman. *Chem. Geol.* **112,** 247–254.
Swart P. K. (1990) Calibration of the ion microprobe for the quantitative determination of strontium, iron, manganese and magnesium in carbonate minerals. *Anal. Chem.* **62,** 722–728.
Treiman A. H. (1995) A petrographic history of martian meteorite ALH84001: Two shocks and an ancient age. *Meteoritics* **30,** 294–302.
Treiman A. H. (1998) The history of Allan Hills 84001 revised: Multiple shock events. *Meteor. Planet. Sci.* **33,** 753–764.
Treiman A. H., Berrett R. A., and Gooding J. L. (1993) Preterrestrial aqueous alteration of the Lafayette (SNC) meteorite. *Meteoritics* **28,** 86–97.
Treiman A. H. and Romanek C. S. (1998) Bulk and stable isotopic compositions of carbonate minerals in Martian meteorite Allan Hills 84001: No proof of high formation temperature. *Meteor. Planet. Sci.* **33,** 737–742.
Utzmann A., Bausch W. M., and Joachimski M. M. (1999) Trace element and stable isotope geochemistry of secondary carbonates in alkaline volcanic rocks of the Rhoen, Germany. *Chem. Erde Geochem.* **59,** 105–121:
Valley J. W., Eiler J. M., Graham C. M., Gibson E., Romanek C., and Stolper E. M. (1997) Low temperature carbonate concretions in the martian meteorite ALH84001: Evidence from stable isotopes and mineralogy. *Science* **275,** 1633–1638.
Valley J. W., Graham C. M., Harte B., Kinny P., and Eiler J. M. (1998) Ion microprobe analysis of oxygen, carbon and hydrogen isotope ratios. In *Reviews in Economic Geology* (eds. M. A. McKibben, W. C. Shanks and W. I. Ridley), Vol. 7, pp. 73–98. Society of Economic Geology.
Veizer J. (1983) Trace elements and isotopes in sedimentary carbonates. In *Carbonates: Mineralogy and Chemistry*(ed. R. J. Reeder), Vol. 11, pp. 265–300. Mineralogical Society of America.
Veizer J., Hinton R. W., Clayton R. N., and Lerman A. (1987) Chemical diagenesis of carbonates in thin sections-ion microprobe as a trace element tool. *Chem. Geol.* **64,** 225–237.
Vicenzi E. P., Tobin K., Heaney P. J., Onstott T. C., and Chun J. (1997) Carbonate in the Lafayette meteorite: A detailed microanalytical study (abstract). *Meteor. Planet. Sci.* **32,** A132–A133.
Warren P. H. (1998) Petrologic evidence for low-temperature, possibly flood evaporitic origin of carbonates in the ALH84001 meteorite. *J. Geophys. Res.* **103,** 16759–16773.
Wentworth S. J. and Gooding J. L. (1994) Carbonates and sulfates in the Chassigny meteorite: Further evidence for aqueous chemistry on the SNC parent planet. *Meteoritics* **29,** 860–863.

APPENDIX

Analytical Methods

A.1. X-Ray Diffraction

Orange carbonate concretions were identified on the faces of millimeter-sized sample fragments, photographed and characterized by FTIR, and removed from the sample surface with the adhesive from a piece of double-sided tape. We resolved before X-ray diffraction experiments on these removed fragments that the white Mg-carbonate and black inclusion-rich rims were too small in any one concretion for separate analysis by our techniques and therefore sampled only orange carbonate cores of concretions, which are sufficiently large to permit the separate analysis of carbonate from different concretions and, as discussed in the text, are known to have exotic chemical compositions that provide a test of their environment of formation. Individual fragments of carbonate (estimated dimensions of 50 to 150 μm in diameter and 20 to 50 μm thick) were removed from the adhesive on the tape surface with a stainless steel scalpel and mounted with Devcon epoxy onto a 125-μm-diameter glass fiber ~1 to 2 cm long.

Each sample was secured in a 5.73-cm-diameter, evacuated Galdolfi (i.e., precessional Debye-Shearer) camera. The samples were rotated at a rate of 1 rotation/60 s over periods of 1 to 96 h, during which they were irradiated with a Cu or Cr source (run at 45 KeV and 20 nA) filtered with Ni (for the Cu source) or vanadium (for the Cr source). Visible diffraction lines on the resulting film were indexed on a manual film reader, and the films were then digitized with a UMAX Power Look transparency scanner; these images were analyzed by the image processing program "X-ray" to determine the relative intensities of the most intense peaks. The relationship between film opacity and X-ray intensity was calibrated by using known peaks in calcite and α-quartz standards. Procedural blanks were made with epoxy and adhesive from the double-sided tape loaded onto a glass fiber, or no sample or fiber whatsoever. Diffraction lines observed in our procedural blanks have been subtracted from the results presented in Table 1. None of these lines was sufficiently close to sample diffraction lines to create interferences. The accuracy of our measurements was assessed by measurement of five standards: α-quartz, calcite, a natural mixture of calcite and magnesite (estimated 1:3 ratio), and a 1:3 synthetic mixture of magnesio-siderite and ankerite. The location of d-spacings in all standards fell within $\pm$0.003 Å (1σ) of their expected location. This is comparable to the reproducibility in our measurement of diffraction line spacings on a given film ($\pm$50 μm). Given the precision of film experiments, and on the basis of these results, we concluded that no internal standard need be mixed with our sample before analysis —an advantage in the handling and analysis of such small samples. The intensity of our ankerite standard relative to our magnesio-siderite standard (i.e., I_{ank}/I_{sid}) was 1.5 (on a molar basis, 3-oxygen stoichiometry), comparable to the value of 1.4 previously observed for $I_{dolomite}/I_{siderite}$ (Initial Reports of the Ocean Drilling Program, Vol. 4, appendix 3).

The minimum relative intensity of a diffraction line in an unknown sample whose intensity could be clearly measured was 13 $\pm$ 1% of the maximum intensity for that sample. Diffracted lines in both samples and standards that were too faint for precise intensity measurement were still clearly visible on the film and measured for d-spacing on a film reader. The faintest lines that were clearly visible in an unknown sample corresponded to a d-spacing that has a nominal relative intensity of 11% in the phase to which we have assigned that diffraction line (siderite; see Section 4, Phase Identification for details). Several lines with nominal intensities of 11% were easily identified visually in several sample films, such that we regard this as an upper bound on our minimum detection limit. The most intense diffraction line expected for that phase but not observed in any of our films has a nominal relative intensity of 6% of the maximum intensity. On the bases of these observations and the ratio I_{ank}/I_{sid}, we estimate our minimum detection limit for ankerite in magnesio-siderite to be $\geq$4 to 8 mol% and for magnesio-siderite in ankerite to be $\geq$8 to 15 mol%. These detection limits indicate that our analysis can determine whether bulk compositions with 0.04 to $0.06 < X_{Ca} < 0.41$ to 0.44 are mixtures of phases corresponding to the ankerite/magnesio-siderite solvus at $\leq$550°C.

After X-ray diffraction experiments, each sample/fiber assembly was removed from the camera, embedded in epoxy, and polished down with 0.3-μm alumina grit to expose a surface of carbonate for electron microprobe analysis. One of the samples (ALH-1) was lost during this stage of preparation and was not measured for chemical composition. This sample resembled all of the others visually and with respect to its FTIR and X-ray diffraction measurements, and we therefore have no reason to suspect that it does not fall within the range of chemical compositions documented in this sample in this and previous studies.

Several factors contributed to our inability to identify some d-spacings in some films, including a relatively intense background on portions of the film corresponding to apparent d-spacings $>$ ~3.5 Å (e.g., the 3.58 Å diffraction line), and failure to resolve some closely adjacent diffraction lines (e.g., 1.73 and 1.74 Å). Reproducibility of closely similar unknown diffraction lines among the different samples averages $\pm$0.004 Å (1σ). This is comparable to the expected uncertainty based on our estimated precision for measurements of diffraction line locations. This level of precision is sufficient to discriminate among carbonate minerals in the Ca-Fe-Mg-Mn system at a level $\geq 10\sigma$. Our precision is also sufficient to allow meaningful comparison with the known compositional variations of unit-cell dimensions with chemistry in the rhombohedral carbonates.

A.2. Electron Microprobe

We analyzed the major element (Ca, Mg, Mn, Fe) compositions of carbonate in ALH84001 with the SX50 electron microprobe at the University of Wisconsin–Madison. Instrumental settings included an accelerating voltage of 15 KeV and a beam current of 6 nA; all measurements were made with a focused electron beam. Natural car-

bonate minerals were used as standards; carbon was determined by difference and oxygen by stoichiometry. The data were reduced by the PAP matrix correction (Pouchou and Pichoir, 1984).

A.3. Ion Microprobe

$^{18}O/^{16}O$ ratios were measured for carbonate, silicate, and oxide phases in ALH84001 with the Cameca ims 4f ion microprobe at the University of Edinburgh. Analyses used a primary beam of Cs^+ ions, an electron flood gun, and a high-energy offset (350 ± 25 eV) for analyzed secondary O^- ions. Other analytical details are reviewed elsewhere (Eiler et al., 1997a; Valley et al., 1998). Four hundred analyses of 12 carbonate standards were made to assess standard homogeneity and instrument stability. Both internal precision defined by counting statistics and point-to-point reproducibility for any one standard in any one analytical session averaged ±1.0‰ (1σ). Two hundred sixteen analyses in 10 analytical sessions permit comparison of instrument fractionation ($\alpha_{SIMS} = {}^{18}O/^{16}O_{measured}/{}^{18}O/^{16}O_{accepted}$) among standard materials. These comparisons were grouped into averages for each material in each session, and all sessions were mutually normalized to a constant value of α for a mineral analyzed in other sessions. The relative differences in α_{SIMS} between any two materials in different analytical sessions had an average reproducibility of ±0.0008 (0.8‰, 1σ, 12 comparisons). We found α_{SIMS} for carbonate standards to be correlated with secondary ion yield, mean atomic weight, and Fe content of Fe-Mg-Ca carbonates. The relationship to Fe content appears simplest and most precise; therefore, we used it as an empirical calibration for correcting raw data on unknown carbonates from ALH84001. A figure showing this calibration is presented in Eiler et al. (1997b). A silicate standard (Amelia albite) was also analyzed in several sessions so that we could tie our carbonate standardization to previously established silicate mineral and glass standardization schemes (Eiler et al., 1997a). Analyses of enstatite and feldspathic glass in ALH84001 were based on comparison with Amelia albite standard and algorithms for standardization silicate materials discussed in Eiler et al. (1997b). We did not have an appropriate standard for calibration of chromite analyses and have corrected them on the basis of extrapolations of relationships between α_{SIMS} and mineral chemistry presented in Eiler et al. (1997b); the corrected values should be regarded as approximate, although external precision of our measurements of this material is not significantly effected by this uncertainty. We estimate that the accuracy of corrections for other unknowns (carbonates, enstatite, and feldspathic glass) have uncertainties of ~1 to 2‰ in addition to the external errors of our measurements. This added uncertainty should have little effect on the reproducibility of our analyses of pyroxene and glass (which are relatively invariant in major-element chemistry) but significantly contribute to point-to-point precision of carbonate analyses. We suggest that the total analytical uncertainty of silicate analyses is ±1‰, whereas those for carbonates are closer to ±2‰ despite similar internal and external precision for silicate and carbonate standards.

The abundances of selected trace elements were measured in 20 spots in carbonates in ALH84001 by secondary ion mass spectrometry with a Cameca ims 4f ion microprobe following techniques modified after Veizer et al. (1987). A 5-nA primary beam of O^- was used with an image field of 25 μm. Secondary ions were collected by using an energy offset of 78 eV. Natural carbonate standards included Norman Cross Calcite (Swart, 1990) for Sr, Ba, Fe, and Mn, and calcite from the Oka Carbonatite for La, Ce, and Nd. The other trace-element concentrations (Rb, B, Th, U, Zr, and Y) were estimated from patterns derived from analysis of NBS-610 glass. Ion yields were measured relative to ^{44}Ca in carbonates and ^{30}Si in the silicate glass standard.

A.4. Infrared Spectroscopy

Reflectance FTIR spectra were obtained on a Nicolet 60sx spectrometer equipped with modified Nicolet 620 data-processing terminal. Samples were introduced to the beam path by placement in a NicPlan microscope, equipped with a sample collar purged with dry air. Two hundred fifty-six scans were signal-averaged to produce a primary spectrum, which was ratioed to a reference spectrum taken of polished Au. Peak positions of the normalized reflectance spectra were determined as the point of minimum change in intensity with variation in wave-number across the peak profile.

A variety of carbonate standards (including calcite, aragonite, dolomite, ankerite, siderite, and magnesite) were measured by these techniques to characterize the location and appearance of absorption features measured in the reflectance mode, which can differ substantially from data collected in transmittance mode. Two of the principal absorption features in carbonate minerals at ~730 cm^{-1} and ~880 cm^{-1}, conventionally designated as ν^2 and ν^4, are identifiable in these spectra at wave numbers approximately corresponding to values observed in transmittance measurements, but systematically offset to higher wave numbers (by 4 to 19 U). We attribute this small, systematic shift to the difference in optical paths between reflectance and transmittance measurements. The wave numbers of ν^2 and ν^4 peaks measured in reflectance mode for our rhombohedral carbonate standards are well correlated with the wave numbers of those peaks previously measured by transmittance FTIR spectroscopy; this relationship was used for comparison of measured locations of ν^2 and ν^4 in orange carbonate from ALH84001 to the known compositional dependence of these peaks based on previous transmittance measurements of rhombohedral carbonates. The third and strongest feature to our measurements was a broad, composite peak including a poorly defined break in slope at 1400 to 1450 cm^{-1} and a more well defined maximum intensity at 1550 to 1580 cm^{-1}. This feature corresponds to the approximate location of the transverse and longitudinal components to the CO_3^- complex stretching in carbonate minerals (ν^3), which is characteristically broad as in our measurements, but centered on a peak at 1400 to 1450 cm^{-1} in transmittance measurements. This feature is less diagnostic of phase identity of rhombohedral carbonates, both because of its broad character and relatively weak compositional dependence, and was not used for detailed comparison of unknown carbonates in ALH84001 to standards.